β-importins Tnpo-SR and Cadmus and the small GTPase Ran promote ovarian cyst formation in *Drosophila*

Allison N. Beachum, Taylor D. Hinnant, Anna E. Williams, Amanda M. Powell, and Elizabeth T. Ables*

Department of Biology, East Carolina University, Greenville, NC 27858.

*Correspondence: ablese@ecu.edu; 1001 E. 10th St. Mailstop 551, Greenville, NC 27858; Phone: 252-328-9770; Fax: 252-328-4178

RUNNING TITLE

importins promote cyst formation

KEYWORDS

Oocyte, oogenesis, germline, cyst, germline stem cell

CORRESPONDING AUTHOR:

Elizabeth T. Ables
East Carolina University
Department of Biology
1001 E. 10th St., Mailstop 551
553 Science & Technology Building
Greenville, NC 27858
Office phone: 252-328-9770
e-mail: ablese@ecu.edu

SUMMARY STATEMENT

Ran and two β-importins function coordinately to promote oocyte selection and cyst development in the *Drosophila* ovary.

ABSTRACT

Germ cells undergo mitotic expansion via incomplete cytokinesis, forming cysts of undifferentiated cells that remain interconnected prior to meiotic initiation, through mechanisms that are not well-defined. In somatic cells, Ras-related nuclear protein (Ran) spatiotemporally regulates mitotic spindle assembly, cleavage furrow formation and abscission. Here, we identify Ran and β-importins as critical regulators of cyst development in the *Drosophila* ovary. Depletion of *Ran* or the β-importins *Tnpo-SR* and *cadmus* disrupts oocyte selection and results in egg chambers with variable numbers of germ cells, suggesting abnormal cyst development and cyst fragmentation. We demonstrate that Ran, Tnpo-SR, and Cadmus regulate key cellular processes during cyst formation, including cell cycle dynamics, fusome biogenesis, and ring canal stability, yet do so independently of mitotic spindle assembly. Further, Tnpo-SR and Cadmus control cyclin accumulation and suppress cytokinesis independent of Ran-GTP, suggesting that β-importins sequester protein cargos that normally promote the mitotic-to-meiotic transition. Our data demonstrates that Ran and β-importins are critical for germ cell cyst formation, a role that is likely conserved in other organisms.

INTRODUCTION

Germ cells develop as cysts of interconnected undifferentiated cells (Lu et al., 2017; Matova and Cooley, 2001; Pepling and Lei, 2018). Cysts arise via incomplete cytokinesis, manifested by cleavage furrow arrest and the formation of stable ring canals that permit transport of cytoplasm and organelles (de Cuevas et al., 1997; Guertin et al., 2002; Haglund et al., 2011; Pepling and Lei, 2018). Cyst formation increases cytoplasmic volume, enhances sensitivity to DNA damage, and ensures robust oocyte development (Chaigne et al., 2020; de Cuevas et al., 1997; Pepling and Lei, 2018; Pepling et al., 1999; Yamashita, 2018). Cyst formation is evolutionarily conserved and essential for optimal fertility in multiple phyla (Haglund et al., 2011; Lu et al., 2017).

The fruit fly, *Drosophila melanogaster*, is an elegant model of germline cyst formation. In adult females, oocytes are produced in a linear spatiotemporal arrangement fueled by the activity of germline stem cells (GSCs; Figure 1A) (Hinnant et al., 2020). GSCs divide asymmetrically, giving rise to one daughter that remains a GSC and a cystoblast that differentiates. Delayed abscission between the GSC and cystoblast keeps the pair connected well into G2 of the subsequent cell cycle (Ables and Drummond-Barbosa, 2013; Eikenes Å et al., 2015; Hinnant et al., 2017; Mathieu et al., 2013; Matias et al., 2015). Cystoblasts divide four times with incomplete cytokinesis, creating 16-cell cysts. At the completion of the mitotic divisions, cleavage furrows between germ cells are modified into stable ring canals (Grieder et al., 2000; Guertin et al., 2002; Hinnant et al., 2020). The fusome, a cytoplasmic organelle composed of microtubules, endoplasmic reticulum-derived vesicles, and membrane skeleton proteins, traverses the intercellular bridges (Hinnant et al., 2020; Ong and Tan, 2010; Pepling and Lei, 2018; Röper, 2007; Snapp et al., 2004). The fusome branches as mitotic divisions progress, providing a synchronization hub for cell cycle regulation and cell polarity (Grieder et al., 2000; Hinnant et al., 2020; Lighthouse et al., 2008). These specialized cytological features of germ cells facilitate interconnectivity and are vital to oocyte selection; however, the molecular mechanisms underlying fusome morphogenesis and incomplete cytokinesis are not well understood.

Formation of an actomyosin-based contractile network at the equatorial cleavage plane during cytokinesis is spatiotemporally regulated and requires a dynamic interplay between the cytoskeleton, the mitotic microtubule-based central spindle, and membrane trafficking (Frémont and Echard, 2018; Haglund et al., 2011; Nguyen and Robinson, 2020; Pollard and O'Shaughnessy,

78 2019). Central to this process is Ras-related nuclear protein (Ran), a small guanosine triphosphate
79 (GTP)-binding protein implicated in protein transport during mitosis and interphase (Ozugergin
80 and Piekny, 2020; Sazer and Dasso, 2000). Ran partners with α- and β-importins to move protein
81 cargo into the nucleus and promote mitotic spindle assembly (Cautain et al., 2015; Okada et al.,
82 2008). Ran also regulates cell polarization and contractile protein localization during cleavage
83 furrow ingression (Beaudet et al., 2017; Silverman-Gavrila et al., 2008). Chromatin-associated
84 Ran-GTP may help recruit and organize essential proteins at the cortex, thereby ensuring the
85 robustness of cytokinesis (Nguyen and Robinson, 2020).

86 Here, we identify Ran and β-importins as novel regulators of germline cyst formation in
87 the *Drosophila* ovary. We show that Ran and β-importins Tnpo-SR and Cadmus (Cdm) control
88 cyst formation by regulating cell cycle dynamics, fusome biogenesis, and ring canal stability. Ran
89 function depends on its active, GTP-bound state, as expression of a dominant-negative *Ran* mutant
90 recapitulates *Ran* loss-of-function. *Ran*, *Tnpo-SR*, and *cdm* are not essential for mitotic spindle
91 assembly in undifferentiated germ cells. Moreover, knock-down of *Tnpo-SR* or *cdm* does not
92 completely phenocopy loss of *Ran*, suggesting that β-importins control cell cycle progression and
93 suppress cytokinesis independent of Ran activity. Given the conservation of germline cyst
94 formation across phyla, our data suggest that Ran and specific β-importins may play similar roles
95 in other organisms.

96

97 **RESULTS**

98 ***RNAi screen reveals that β-importins and Ran are essential for germ cell development.***

99 We previously identified *Transportin-Serine/Arginine rich* (*Tnpo-SR*) in a genetic mosaic
100 screen for genes controlling GSC self-renewal (Ables et al., 2016). *Tnpo-SR*, homologous to
101 mammalian *TNPO3*, encodes a β-importin (Allemand et al., 2002; Lai et al., 2001). To determine
102 whether *Tnpo-SR* loss-of-function phenotypes reflect a general role for importins in germ cell
103 mitoses, we performed a secondary reverse genetic screen using germline-enhanced RNA
104 interference (RNAi) to knock-down expression of nine *Drosophila* importins and the small
105 GTPase *Ran* specifically in germ cells (Figure 1B-D, Table 1) (Ni et al., 2011; Rørth, 1998; Van
106 Doren et al., 1998). In contrast to driver-only controls (Figure 1B, Table 1), three RNAi lines
107 produced completely agametic ovaries, defined by the absence of egg chambers (Figure 1C). More
108 intriguingly, four RNAi lines corresponding to *Ran* and the β-importins *Tnpo-SR*, *cadmus* (*cdm*),

109 and *Fs(2)Ket* (also called *Ketel*) exhibited a partial agametic phenotype, in which germ cells were
110 present in some ovarioles, but in unusually shaped egg chambers (Figure 1D; Table 1). Cdm and
111 Tnpo-SR are paralogs, sharing 42% amino acid similarity, while Ketel is less conserved. These
112 results demonstrate that Ran and some β-importins are necessary for proper oocyte development
113 and may have distinct functions.

114 Since GSCs give rise to all germ cells, we hypothesized that agametic ovaries resulting
115 from *Ran* and *β-importin* knock-down could arise from a failure to establish or maintain GSCs. To
116 test this, we quantified the number of GSCs per germarium. GSCs and their progeny can be easily
117 identified by immunolabeling of Hts, a fusome-resident protein in germ cells, and LaminC
118 (LamC), a nuclear envelope protein highly expressed in cap cells (the major cellular component
119 of the GSC niche) (Ables and Drummond-Barbosa, 2013). Unlike cytoblasts, GSCs possess an
120 anteriorly localized fusome juxtaposed to the cap cells (de Cuevas and Spradling, 1998; Lin et al.,
121 1994). All four partially agametic RNAi lines had significantly less GSCs per germarium at three
122 days after eclosion than age-matched driver-only controls (Table 1; Supp. Figure 1A-C). Fewer
123 GSCs in early adulthood suggests that *Ran*, *Tnpo-SR*, *Ketel*, and *cdm* are required for GSC
124 establishment during larval/pupal development or during the proliferative surge in GSCs following
125 the female's first mating (Ameku and Niwa, 2016; Van Doren et al., 1998). Conditional knock-
126 out of *Tnpo-SR* further demonstrated the requirement for β-importin function in GSC maintenance.
127 We used two strong loss-of-function transposon insertion alleles of *Tnpo-SR* (*Tnpo-SR*^{KG04870} and
128 *Tnpo-SR*^{LL05552}) carrying *FRT* sites to generate germline mutant mosaic germaria under the
129 *Flippase* (*FLP*)/*FLP Recognition Target* (*FRT*) genetic mosaic lineage-tracing system (Laws and
130 Drummond-Barbosa, 2015; Xu and Rubin, 1993). GFP-negative GSC clones were generated at
131 equivalent rates in control, *Tnpo-SR*^{KG04870}, and *Tnpo-SR*^{LL05552} mosaic germaria at four days after
132 clone induction (Supp. Figure 1F). In contrast to mock controls, *Tnpo-SR*^{KG04870} and *Tnpo-SR*^{LL05552}
133 germline mutant mosaic germaria rapidly lost marked GSCs over time (Supp. Figure 1D-F),
134 indicating that *Tnpo-SR* is cell-autonomously required for GSC self-renewal.

135

136 ***Loss-of-function mutations in Ran and β-importins alter the number of germ cells per egg***
137 ***chamber.***

138 The intriguing phenotype resulting from knock-down of *Ran* and β-importins prompted us
139 to examine egg chamber morphology more closely. To visualize germline and follicle cells, we

140 combined anti-Hts antibodies with anti-Hts-RC antibodies, which are specific for a Hts cleavage
141 product that localizes to ring canals (Petrella et al., 2007; Robinson et al., 1994). Unlike driver
142 control egg chambers (Figure 1E; Table 1), knock-down of *Ran*, *cdm*, or *Tnpo-SR* significantly
143 decreased the number of egg chambers with 16 germ cells (Figure 1F-G; Table 1). Depletion of
144 *Ketel* did not significantly impact egg chamber formation (Table 1).

145 Cystoblasts normally divide synchronously four times, following a 2^n pattern, to produce
146 cysts with 16 cells (King, 1970). To determine whether extra germ cells in *Ran*, *cdm*, and *Tnpo-*
147 *SR* depleted ovarioles arose by alterations in the number of mitotic divisions, we quantified the
148 number of germ cells per cyst (Figure 1J). In the rare instances where control or *Ketel* RNAi egg
149 chambers had an abnormal number of germ cells, they invariably contained 32 cells (Figure 1J).
150 In contrast, knock-down of *Ran*, *cdm,* or *Tnpo-SR* produced egg chambers with variable numbers
151 of germ cells, ranging anywhere from one to 49 cells per cyst (Figure 1J). While some egg
152 chambers housed germ cells on the order of 2^n, a substantial number deviated from this pattern
153 (Table 1). Germ cell numbers in adjacent chambers in RNAi-depleted egg chambers did not add
154 up to 8, 16, or 32 cells, arguing that encapsulation defects alone are not the source of the unusual
155 germ cell number phenotype. Some egg chambers with 32 or more cells had oocytes with five ring
156 canals, suggesting that some abnormal egg chambers arose by an extra mitotic division. Other egg
157 chambers, however, likely arose because of other cellular defects. Moreover, a small percentage
158 of *cdm* and *Tnpo-SR* RNAi knock-down ovarioles (17.4% and 13.3% of all ovarioles, respectively)
159 contained germline tumors, in which a normal follicle cell monolayer surrounded mitotically-
160 active germ cells with underdeveloped fusomes (Figure 1H-I; Supp. Figure 2A-C'). In *Tnpo-SR*
161 RNAi ovarioles, undifferentiated germ cells were encapsulated with more-developed germ cells
162 (Supp. Figure 2A). Germline tumors contained mitotically-active cells with short or unbranched
163 fusomes and immature ring canals that frequently appeared as dot-like structures, reminiscent of
164 the abscission site in GSC/cystoblast pairs (Supp. Figure 2B-C'). These structures suggest tumors
165 arose because of improper abscission events in 2-cell and/or 4-cell cysts. Immunostaining for Sex-
166 lethal (Sxl), which is enriched in GSCs and cystoblasts in the anterior-most region of the
167 germarium (Supp. Figure 2D-D') (Chau et al., 2009), confirmed that *Tnpo-SR* RNAi germ cells
168 have not completed differentiation (Supp. Figure 2E-E'). We conclude that Ran, Tnpo-SR, and
169 Cdm impact the synchrony and number of cyst divisions.
170

171 ***Ran, Tnpo-SR, and cdm are required for oocyte selection.***

172 During germ cell mitotic divisions, three to four cyst cells initiate meiosis by assembling
173 the synaptonemal complex; however, only one of these cells is maintained as the oocyte (Hughes
174 et al., 2018). Since depletion of *Ran*, *Tnpo-SR*, or *cdm* altered the number of germ cells per cyst,
175 we hypothesized that oocyte selection was also affected. In wild-type egg chambers just posterior
176 to the germarium, the oocyte-specific proteins Orb (Figure 2A) and Bicaudal D (BicD) (Figure
177 2D) had clearly accumulated in one posterior cyst cell. In contrast, egg chambers from germline-
178 depleted *Ran*, *Tnpo-SR*, or *cdm* females did not properly express Orb (*Ran*^{GL01341}*, cdm*^{HMS02846}*, and*
179 *Tnpo-SR*^{V22}) or BicD (*Tnpo-SR*^{V22}) (Figure 2B-C,E-F; Table 1). Many loss-of-function egg
180 chambers also lacked a cell with a karyosome, a clear indicator of oocyte fate (Figure 3B-C,E-F).
181 Importantly, most of the *nos-Gal4>Ran*^{GL01341} and *nos-Gal4>cdm*^{HMS02846} egg chambers with 16
182 germ cells contained an oocyte (Table 1), suggesting that loss of oocyte identity is a secondary
183 effect of incorrect mitotic divisions in the absence of *Ran* and *cdm*. This was not the case, however,
184 for *Tnpo-SR*, as 34% of *nos-Gal4>Tnpo-SR*^{V22} egg chambers with 16 germ cells contained only
185 nurse cells (Table 1). Similarly, in *Tnpo-SR* germline mutant mosaic germaria, mutant cysts
186 located posterior to wild-type cysts (thus at a more advanced stage of development) failed to up-
187 regulate Orb expression to similar levels as adjacent wild-type cysts (Figure 2G-H). Further, a core
188 component of the synaptonemal complex, C(3)G, normally present as early as the 4-cell cyst stage,
189 did not accumulate in *Tnpo-SR*^{KG04870} mutant cysts to equivalent levels as adjacent wild-type cysts
190 (Figure 2I-J). This suggests that *Tnpo-SR* is specifically required for oocyte specification
191 independent of its role in cyst divisions.

192

193 ***Ran is dynamically localized in cyst cells and dispensable for spindle assembly.***

194 One well-characterized function of Ran and β-importins is the regulation of spindle
195 assembly (Cesario and McKim, 2011; Forbes et al., 2015; Nguyen and Robinson, 2020; Ozugergin
196 and Piekny, 2020). Spindle orientation is critical for GSC maintenance, and mitotic spindle
197 remnants accumulate in fusomes as cysts divide (Cheng et al., 2008; Deng and Lin, 1997; Grieder
198 et al., 2000; Máthé et al., 2003). Like other small GTP-binding proteins, Ran cycles between active
199 (GTP-bound) and inactive (GDP-bound) states (Ozugergin and Piekny, 2020). Ran-GTP
200 dissociates importin-bound cargo in the nucleus and is converted to Ran-GDP in the cytoplasm. In
201 some cell types, this establishes a gradient of active Ran in the cell that promotes spindle formation.

202 To determine whether such a gradient may exist in cyst cells, we first analyzed the
203 subcellular distribution of Ran. We took advantage of a previously characterized transgene in
204 which the germline-specific *UASp* promoter drives an N-terminal hemagglutinin (HA)-tagged Ran
205 (Ran^{HA}) (Cesario and McKim, 2011). Using *nos-Gal4* to drive Ran^{HA} in germ cells, we then
206 localized Ran using anti-HA antibodies in comparison to mitotic spindles (labeled with α-tubulin),
207 fusomes, and chromosomes (Figure 4A-A'). Unlike neuroblasts, in which Ran-HA is nuclearly
208 localized during interphase and overlaps with the mitotic spindle during mitosis (Cesario and
209 McKim, 2011), we did not observe strong nuclear localization of Ran-HA in GSCs or cyst cells
210 (Figure 3A-B''). Ran-HA was higher in the cytoplasm than in nuclei of interphase and mitotically-
211 active cells and, consistent with neuroblasts and embryonic cells (Cesario and McKim, 2011;
212 Trieselmann and Wilde, 2002), was absent from chromosomes (Figure 3B-B''). Ran-HA
213 expression was higher in some cysts than others, likely due to minor variations in driver strength.
214 In contrast to meiotic spindles (Cesario and McKim, 2011), we did not observe strong
215 accumulation of Ran-HA surrounding mitotic spindles (Figure 3B-B'').

216 We then asked whether Ran-GDP accumulated in specific subcellular locations in cyst
217 cells. We over-expressed an HA-tagged Ran^{T24N}, which carries an amino acid substitution that
218 locks Ran into a GDP-bound state and inhibits cargo loading (Cesario and McKim, 2011; Drutovic
219 et al., 2020). As expected, Ran-GDP was primarily cytoplasmic in interphase cells (Figure 3C).
220 We also observed that Ran-GDP accumulated in the nucleus of mitotically-dividing cells (Figure
221 3C), overlapping with chromatin at metaphase (Figure 3D-D''). Mitotic spindles appeared to
222 assemble correctly (see below), but chromatin was dispersed in interphase cells.

223 The subcellular localization of Ran-GTP was markedly different than that of Ran-GDP.
224 We used a second HA-tagged transgene, Ran^{Q69L}, to over-express a constitutively active form of
225 Ran locked in a hydrolysis-resistant GTP-bound state (Cesario and McKim, 2011). Ran-GTP was
226 excluded from cyst cell nuclei during interphase (Figure 3C) and accumulated at the presumptive
227 nuclear membrane during mitosis (Figure 3D-D''). Taken together, these experiments suggest that
228 Ran aids in chromatin condensation or cytokinesis following the completion of mitosis.

229 Finally, we asked whether Ran and β-importins are necessary for spindle formation. Using
230 immunostaining for α-Tubulin, we confirmed that mitotic spindles in dividing cysts are anchored
231 to the fusome, oriented perpendicularly (Figure 3G) (Megraw and Kaufman, 2000; Storto and
232 King, 1989). Surprisingly, in *cdm*-depleted (Figure 3H) or *Tnpo-SR*-depleted (Figure 3I) germ

233 cells, similar-sized spindles formed and were appropriately anchored and oriented with respect to
234 fusomes. Similarly, we were unable to find defects in spindle formation or orientation in
235 *nosGal4>Ran*^{T24N} germ cells (Figure 3D,J). We conclude that mitotic spindles can form even when
236 Ran-GTP is depleted, suggesting that low levels of active Ran are sufficient to maintain germ cell
237 mitoses.
238
239 ***GSC establishment, cyst formation, and oocyte selection require active Ran-GTP.***
240 Given the intriguing localization of Ran-GTP, we then asked whether active Ran-GTP is
241 required for GSC establishment and cyst formation. Flies expressing the *Ran*^{T24N} and *Ran*^{Q69L}
242 mutations in germ cells were compared to flies expressing wild-type *Ran*^{HA}. We expected that
243 constitutively expressing Ran-GDP would titrate out the amount of active Ran, thus mimicking
244 *Ran* loss-of-function. Indeed, over-expression of *Ran*^{T24N} resulted in a partial agametic phenotype
245 and the average number of GSCs per germarium was substantially reduced as compared to age-
246 matched controls (Figure 4A; Table 1). Over-expression of dominant negative *Ran*^{T24N} also altered
247 the number of germ cells per cyst (Figure 4B-C,E) and, similar to knock-down of *Ran* via RNAi,
248 the number of germ cells did not always follow a 2^n pattern (Figure 4E, Table 1). Over-expression
249 of *Ran*^{T24N} also impaired oocyte selection, as 12-24% of egg chambers with 16 germ cells lacked
250 an Orb-positive cell (Table 1). These phenotypes are consistent with depletion of *Ran* via RNAi
251 and likely contribute to the female sterility phenotype noted in prior studies (Cesario and McKim,
252 2011).
253 Intriguingly, excess Ran-GTP in germ cells did not result in severe germline defects
254 (Figure 4D-E, Table 1). The average number of GSCs per germarium was slightly reduced in *nos-*
255 *Gal4>Ran*^{Q69L} ovarioles (Table 1) and a few egg chambers had an incorrect number of cells (Figure
256 4E), but defects were not as severe or penetrant as either the *Ran* RNAi or Ran-GDP-locked
257 mutants. Since we did not observe a clear Ran intracellular concentration gradient or accumulation
258 of Ran at mitotic spindles, these results suggest that Ran-GTP levels are already in excess in
259 mitotically-active germ cells, perhaps to facilitate timely mitotic divisions.
260
261 ***Tnpo-SR and cdm, but not Ran-GTP, are required for fusome biogenesis and maturation.***
262 The fusome extends through ring canals during incomplete cytokinesis, forming an
263 extensive tubular network whose structure changes over the course of the mitotic divisions

264 (Lighthouse et al., 2008; Röper, 2007; Snapp et al., 2004). The cytoskeletal core is prominent in
265 GSC and cystoblast fusomes, but is replaced with endoplasmic reticulum-like vesicles as cysts exit
266 the germarium (Figure 5A) (Röper, 2007). Loss of *Hts*, a core fusome cytoskeletal protein, alters
267 the number of germ cells per cyst (Yue and Spradling, 1992). Since knock-down of *Ran* or the β-
268 importins produced similar phenotypes, we hypothesized that abnormal fusome morphogenesis
269 might abrogate cyst formation. Using Hts immunostaining as an indicator of fusome morphology,
270 we observed that when *cdm* (Figure 5B) or *Tnpo-SR* (Figure 5C and Supp. Figure S3) were
271 depleted, germ cells formed long, thin fusomes with irregular branching, particularly in cysts in
272 the middle to posterior third of germaria. Fusomes in *Tnpo-SR*- and *cdm*-depleted germ cells often
273 had thread-like sections separated by thicker sections, consistent with weak points in the
274 cytoskeletal structure (Figure 5B-C). Irregular fusomes were also observed in *Tnpo-SR*-depleted
275 GSC/cystoblast pairs, where new fusome material builds from the cystoblast to the GSC (compare
276 Figure 5E-F) (de Cuevas and Spradling, 1998). Importantly, we did not observe fusomes
277 connecting GSCs to other cyst cells in stem-cysts, as was reported for germ cells in which the
278 chromosomal passenger complex, which regulates abscission timing in GSCs, is abrogated
279 (Mathieu and Huynh, 2017). We also did not observe GSCs or cysts with asynchronous mitoses
280 (compare Figure 5G-H), as we would predict if fusomes lost complete connectivity between cells.
281 We conclude that *Tnpo-SR* and *cdm* promote fusome maintenance or remodeling.

282 To further investigate how the importins regulate fusome morphogenesis, we recombined
283 the *Tnpo-SR*^{V22} RNAi transgene with two fluorescently tagged fusome-resident protein reporters.
284 *Scribble* (*scrib*) encodes a scaffolding protein that regulates vesicle trafficking and is expressed at
285 the cell cortex and in immature fusomes of GSCs and dividing cysts (Figure 5I) (Lighthouse et al.,
286 2008). By the third mitotic division, *Scrib-GFP* is largely absent from wild-type fusomes and does
287 not co-localize with Hts in 16-cell cysts. In *Tnpo-SR*-depleted germ cells, *Scrib-GFP* was
288 prominently expressed in the long, thin fusomes of germ cells in the posterior of germaria (Figure
289 5J). Conversely, Reticulon-like1 (Rtnl1) is an endoplasmic reticulum-resident protein that is
290 expressed in low levels in immature fusomes (Figure 5K) (Röper, 2007). *Rtnl1-GFP* becomes
291 enriched in mature fusomes coincident with cyst division and inversely correlated with Hts
292 expression, reaching peak concentration in fusomes after the final mitotic division (Figure 5K).
293 When *Tnpo-SR* is depleted, *Rtnl1-GFP* and Hts co-localize in fusomes throughout the posterior of
294 the germarium (Figure 5L). These data suggest that in the absence of β-importins, cytoskeletal

295 components of the fusome fail to degrade properly, maintaining the fusome in an immature state
296 that is weakly connected between cyst cells. Intriguingly, fusome shape and branching in cysts
297 over-expressing the dominant negative *Ran*^{T24N} mutant (Figure 5D) were indistinguishable from
298 wild-type cysts, suggesting that Cdm and Tnpo-SR regulate fusome morphogenesis independently
299 of Ran-GTP.
300
301 ***Tnpo-SR and cdm promote cyst formation by suppressing cytokinesis.***
302 Knock-down of *Tnpo-SR* or *cdm* produced egg chambers variable numbers of germ cells;
303 however, it remained unclear to us exactly how such egg chambers could arise. Key observations
304 came by closely examining the morphology of *Tnpo-SR* mutant cysts surrounded by wild-type
305 cysts in mutant mosaic germaria. While knock-down of *Tnpo-SR* by RNAi led to >16 germ cells
306 per egg chamber, we only rarely found examples of *Tnpo-SR*^{KG04870} or *Tnpo-SR*^{LL05552} mutant egg
307 chambers with more than 16 mutant germ cells. We did find, however, compound egg chambers
308 in which a *Tnpo-SR* mutant cyst was encapsulated together with wild-type cysts (Supp. Figure
309 S3A). We occasionally identified mitotically-dividing *Tnpo-SR*^{KG04870} and *Tnpo-SR*^{LL05552} mutant
310 germ cells in mosaic egg chambers outside of the germarium, which never occurs in wild-type
311 germ cells (Supp. Figure S3B). We also frequently found clusters of single *Tnpo-SR* mutant germ
312 cells at the posterior of germaria (Supp. Figure S3C,E-E'''), suggesting that some cyst defects in
313 *Tnpo-SR* mutant and RNAi-knock-down ovarioles could arise by cyst fragmentation. In the *Tnpo-*
314 *SR* RNAi model, where all germ cells lack appropriate Tnpo-SR levels, fragmented cysts would
315 likely be encapsulated along with adjacent cysts, thus yielding irregular (i.e., not 2^n) numbers of
316 germ cells per cyst. In support of this idea, we observed examples of mutant mosaic germaria in
317 which *Tnpo-SR*^{KG04870} mutant cells with dot-like fusomes were adjacent to one another with
318 fusomes aligned along the same plane, as if they were connected (Supp. Figure S3D).
319 Immunostaining with anti-pTyr antibodies to visualize ring canals highlighted *Tnpo-SR*^{KG04870}
320 mutant cysts where ring canal components accumulated on adjacent cyst cells, separated by a very
321 thin line of GFP-positive cytoplasm (Figure 6A and Supp. Figure S3E), suggesting that cells have
322 physically separated from each other after clone induction. Moreover, *Tnpo-SR*^{KG04870} mutant germ
323 cells failed to accumulate proper levels of the cell adhesion protein E-cadherin between germ cells,
324 as occurs in adjacent wild-type 16-cell cysts following the final mitotic division and prior to follicle
325 cell encapsulation (Figure 6B) (Fichelson et al., 2010).

326 These data raised the possibility that in the absence of *Tnpo-SR*, cysts fail to stay connected
327 by intercellular bridges, and instead break apart at unstable ring canals. Initially, this seemed
328 unlikely, as our analyses of *Ran*, *cdm*, and *Tnpo-SR* RNAi and *Ran* dominant-negative germ cells
329 focused on egg chambers outside of the germarium, where ring canals containing Hts-RC (a
330 constituent protein of mature ring canals) were easily detected (Figure 1E-G). Moreover, the
331 number of ring canals scaled to the number of germ cells, suggesting that ring canals formed at
332 successive divisions. Spatiotemporal comparison of ring canal formation, however, demonstrated
333 that while Hts-RC is expressed in germ cells from *nos-Gal4>Tnpo-SR*^{V22} ovarioles, its
334 accumulation at ring canals is drastically delayed, such that protein levels are much lower than in
335 age-matched wild-type cysts (compare Figure 6C and D). Similarly, germ cells depleted of *cdm*
336 (Figure 6F) or *Tnpo-SR* (Figure 6G), failed to accumulate pTyr-reactive material (one of the first
337 indicators of ring canal maturation) to wild-type levels in 16-cell cysts. In contrast, ring canal
338 maturation proceeded normally in *Ran*^{T24N} mutant cysts (Figure 6H), supporting the model that
339 Tnpo-SR and Cdm, but not Ran-GTP, stabilize germ cell intercellular bridges, maintaining proper
340 cyst formation (Figure 6M).
341 We then performed immunostaining for Anillin, an actin/myosin-binding protein known to
342 be a β-importin cargo (Beaudet et al., 2017; Beaudet et al., 2020; Chen et al., 2015; Piekny and
343 Maddox, 2010; Silverman-Gavrila et al., 2008). Anillin localization in ring canals begins at the
344 third mitotic division (Figure 6I) (Goldbach et al., 2010; Haglund et al., 2010). In *Tnpo-SR*-
345 depleted germ cells, we observed Anillin deposition within the intercellular bridge, rather than on
346 surrounding rings (Figure 6J). In contrast, Anillin localizes properly to the ring canals in *Ran*^{T24N}
347 mutants (Figure 6K) and occasionally co-localized with the fusome (Figure 6L), supporting the
348 model that Tnpo-SR suppresses cytokinesis in dividing cysts independently of Ran-GTP.
349 Intriguingly, over-expression of a GFP-tagged Anillin in which a nuclear localization signal has
350 been mutated did not alter Anillin localization in abscising GSC/CB pairs (Supp. Figure 4A-B) or
351 at ring canals (Supp. Figure 4C-D), and did not change the number of germ cells per cyst. Although
352 we cannot exclude the possibility that Tnpo-SR may bind Anillin at another protein domain, we
353 speculate that Tnpo-SR indirectly regulates Anillin by binding other cargo proteins that impact
354 Anillin localization.
355
356 ***Ectopic CycA accumulates in Tnpo-SR- and cdm-depleted germ cells.***

357 The cell cycle is tightly regulated to coordinate cyst formation. For example, loss of
358 function of the mitotic cyclin CycB produces cysts with eight cells, while over-expression of CycA
359 or CycE produces cysts with 32 cells (Lilly et al., 2000; Mathieu et al., 2013; Morris et al., 2005;
360 Ohlmeyer and Schüpbach, 2003). CycA and CycB accumulate at the fusome and phosphorylation
361 of CycB by AuroraB Kinase promotes abscission between GSC/cystoblast pairs (Lilly et al., 2000;
362 Mathieu et al., 2013). Given the phenotypic parallels, we hypothesized that Tnpo-SR and Cdm
363 might regulate cyclin dynamics in dividing germ cells. We confirmed that CycA accumulates at
364 the fusome in ~10% of mitotically dividing cysts, but never associates with the fusome of 16-cell
365 cysts in wild-type tissue (Figure 7A,F). *Ran* depletion in *nos-Gal4>Ran*^{GL01341} germaria did not
366 alter CycA kinetics (Figure 7B,F). In contrast, nearly 40% of mitotically-dividing cysts in *Tnpo-*
367 *SR* and *cdm*-depleted germ cells expressed CycA; moreover, CycA expression was observed in the
368 fusomes of 16-cell cysts at an equivalent rate as dividing cysts, suggesting that germ cells remain
369 mitotic (Figure 7C-D,F).
370 As the highest peak of CycB expression occurs following CycA degradation (Morris et al.,
371 2005), we then asked whether CycB regulation was likewise impacted by loss of the β-importins.
372 We utilized the *Drosophila* Fluorescence Ubiquitin-based Cell Cycle Indicator system (Fly-
373 FUCCI) (Zielke et al., 2014) to ask whether CycB expression was altered in the absence of *Tnpo-*
374 *SR*. Importantly, we used a version of the *UASp-CycB-RFP* transgene that includes a canonical
375 nuclear localization sequence (Hinnant et al., 2017; Zielke et al., 2014). When *Tnpo-SR* was
376 depleted, the *UASp-CycB-RFP* localized to germ cell nuclei; however, significantly fewer
377 mitotically dividing cysts expressed CycB as compared to wild-type controls (Figure 7E,G). Taken
378 together, these data suggest that *Tnpo-SR*, and likely *cdm*, promote proper cyclin dynamics in germ
379 cells, maintaining cysts in the mitotic expansion phase and facilitating coordination between cyst
380 division and fusome morphogenesis.
381
382 **DISCUSSION**
383 During germline cyst formation, cell cycle transitions are precisely controlled to promote
384 mitotic divisions and block cellular abscission. Our study adds new details to our understanding
385 of the molecular regulation of germ cell mitotic expansion, identifying previously undescribed
386 roles for β-importins and the small GTPase Ran in mitotic cell cycle exit during cyst formation.
387 Remarkably, we do not detect a clear cytoplasmic-to-nuclear gradient of Ran protein localization

388 in germ cell nuclei. Nor do we find defects in mitotic spindle assembly, cell size, or DNA
389 condensation in the absence of β-importins or activated Ran. Instead, our data suggest that
390 importins and Ran-GTP promote mitotic exit by distinct, yet complimentary mechanisms. We
391 propose the model that Ran-GTP drives germ cell mitoses by mobilizing cell cycle factors,
392 functioning together with the β-importins Tnpo-SR and Cdm to facilitate transport of cell cycle
393 factors from the fusome to other parts of the cell. We propose that independent of Ran, Tnpo-SR
394 and Cdm sequester cell cycle regulators like CycA and Anillin, titrating the levels of protein
395 accessible to Ran-GTP, counterbalancing mitotic progression. Thus, in the absence of Tnpo-SR or
396 Cdm, CycA levels accumulate, causing germ cells to continue in a proliferative state and impairing
397 fusome stability, ring canal maturation, and oocyte terminal differentiation.
398
399 ***Importins may exhibit non-redundant functions in the Drosophila germline.***
400 Although several α-importins have been implicated in oogenesis prior to our study (Geles
401 and Adam, 2001; Mason et al., 2002; Máthé et al., 2000), our study is the first to identify specific
402 roles for β-importins in mitotic expansion. Our data generally support the hypothesis that specific
403 importins regulate distinct aspects of germ cell development (Hogarth et al., 2005; Loveland et al.,
404 2015; Mihalas et al., 2015). We cannot exclude the possibility, however, that RNAi was not
405 sufficient to completely inhibit importin function. For example, Ketel localizes at the nuclear
406 envelope in early embryos and dividing germ cells (data not shown) (Lippai et al., 2000; Tirián et
407 al., 2000; Trieselmann and Wilde, 2002; Villányi et al., 2008), yet we did not observe germ cell
408 mitotic defects in *Ketel*-depleted germ cells. Future studies will need to employ other loss-of-
409 function approaches to test the roles of Ketel and other β-importins more thoroughly.
410 The repertoire of cargo carried by a β-importin determines its role in biological processes
411 and its redundancy with other importins (Kimura and Imamoto, 2014). Although the full extent of
412 protein-protein interactions mediated by Tnpo-SR remains unknown, structural studies indicate
413 that TNPO3 binds proteins involved in chromatin organization, mRNA and protein modification,
414 cell cycle control, and cell-cell communication (Kimura et al., 2017; Maertens et al., 2014). Tnpo-
415 SR is also likely to bind a broad range of cargo proteins, including SR-rich RNA binding proteins.
416 Indeed, Tnpo-SR physically interacts with several proteins essential for mRNA splicing and
417 transport (Allemand et al., 2002). Given that SR-rich proteins facilitate diverse RNA processing
418 events, there are many potential Tnpo-SR cargo proteins that could influence cyst formation and

419 GSC self-renewal, which are heavily influenced by translational control (Bradley et al., 2015;
420 Teixeira and Lehmann, 2019). Our future studies will seek to identify Tnpo-SR and Cdm-
421 interacting proteins, which should provide additional mechanistic details regarding how importins
422 regulate germ cell mitotic expansion.
423
424 ***The number of cyst divisions is regulated by Ran-GTP and β-importins.***
425 Precise spatiotemporal control over cell cycle regulators underlie the transition to the
426 oocyte fate. In support of this, the mitotic cyclin CycA is clearly critical to support differentiation.
427 Failure to degrade CycA leads to self-renewal failure in GSCs, and extra mitotic divisions and loss
428 of oocyte identity in cyst cells (Chen et al., 2009; Ji et al., 2017; Lilly et al., 2000; Morris et al.,
429 2005; Ohlmeyer and Schüpbach, 2003; Sugimura and Lilly, 2006). Moreover, the deubiquitinase
430 encoded by *bag of marbles* (*bam*), one of the few known differentiation factors in *Drosophila* germ
431 cells, is necessary for the transition from GSC to cystoblast and for cystoblast divisions, at least in
432 part because it stabilizes CycA expression in dividing cysts (Ji et al., 2017). CycA/Cdk1 activity
433 is very high in early cyst divisions but decrease as cysts approach the terminal mitotic division
434 (Hinnant et al., 2017; Lilly et al., 2000). Since cystoblasts divide exactly four times, prior studies
435 posited the model that cystoblasts autonomously limit the number of divisions through a molecular
436 counting mechanism that involves Bam, CycA, and the fusome (Hinnant et al., 2020; Huynh, 2006;
437 Ji et al., 2017; King, 1970; Lilly et al., 2000; McKearin, 1997). While a counting mechanism would
438 limit the number of mitotic divisions, it must also promote modification of contractile ring proteins
439 to block cytokinesis, stabilize intercellular bridges into stable ring canals, and maintain the
440 biosynthesis of the fusome (McKearin, 1997).
441 We suggest that the Ran/β-importin intracellular transport system is integrated into the
442 CycA-dependent cell division counting machinery. Depletion of *Ran*, *cdm*, or *Tnpo-SR* generated
443 egg chambers with abnormal numbers of cells (Table 1), some on the order of 2^n reminiscent of
444 cyclin mutants (Lilly et al., 2000; Mathieu et al., 2013; Morris et al., 2005; Ohlmeyer and
445 Schüpbach, 2003), and others deviating from this pattern, more similar to mutants which disrupt
446 intercellular bridge formation and fusome biogenesis (de Cuevas et al., 1996; Lin et al., 1994; Yue
447 and Spradling, 1992). Although we cannot establish a clear temporal sequence of events mediated
448 by Ran from our current data, we envision two possible mechanisms of action. We favor the
449 hypothesis that Ran mediates intracellular movement of CycA itself or a factor that promotes CycA

450 degradation. Binding by Tnpo-SR or Cdm could sequester the cell cycle regulator, preventing
451 activation by sterically inhibiting interaction with a kinase or by blocking protein accumulation at
452 the fusome. High levels of Ran-GTP levels would promote release of the Tnpo-SR cargo, freeing
453 it for activation. In the absence of Tnpo-SR or Cdm, where mitotic regulators cannot be delivered
454 to Ran, CycA levels instead accumulate at the fusome and in the cytoplasm, promoting continued
455 mitotic division. Alternatively, Ran-GTP could regulate contractile protein localization and cell
456 polarization, as has been demonstrated for human Ran in mammalian somatic cells (Beaudet et al.,
457 2017; Silverman-Gavrila et al., 2008).
458
459 ***Tnpo-SR and Cdm may have Ran-independent roles in promoting cyst development.***
460 Given the close association between Ran and β-importins, we hypothesized that depletion
461 of *Ran* by RNAi, or over-expression of dominant negative Ran^{T24N} mutant would phenocopy β-
462 importin depletion. Yet we observed phenotypes unique to loss of *Tnpo-SR* and *cdm*. In *Tnpo-SR*-
463 and *Cdm*- depleted germ cells, delayed maturation of the fusomes and ring canals appears to create
464 weak connections between cells, resulting in premature abscission or collapsed intercellular
465 bridges (Figure 6M). Interestingly, we see fusomes that are fragile and unbranched (Figure 5E-H),
466 but also germline tumors containing cells with immature fusome morphology resembling that of
467 2-cell cysts (Figure 2G-H). This may be the result of altered timing or different concentrations of
468 the β-importins in the first division of the cystoblast versus the remaining three, perhaps reflecting
469 differing sensitivity to abscission across the mitotic divisions (Mathieu et al., 2013; McKearin and
470 Ohlstein, 1995). Cyst cell fusomes are composed of endoplasmic reticulum-like vesicles and
471 cytoskeletal elements that originate from remnants of the mitotic spindle midbody (de Cuevas and
472 Spradling, 1998; Koch and King, 1966; Koch et al., 1967; Lin and Spradling, 1995; Mahowald,
473 1971). This suggests Ran-independent functions of Tnpo-SR and Cdm in mitotically dividing
474 germ cells, perhaps by sequestering negative regulators of fusome maturation or cytokinesis. We
475 speculate that Tnpo-SR and Cdm promote reorganization of the germ cell cytoskeleton after
476 mitotic division, perhaps by shuttling cytoskeletal proteins back to the fusome.
477
478 ***Ran-GTP and β-importins may function as a conserved molecular timer for the mitotic-to-***
479 ***meiotic transition.***

480 The basic steps in cyst formation have been well described at the morphological level,
481 particularly in insects (de Cuevas et al., 1997; Lu et al., 2017; Pepling and Lei, 2018; Yamashita,
482 2018). Yet how cyst formation is guided molecularly remains an open area for study. Insects
483 provide excellent models, as many exhibit unique mechanisms for achieving cyst formation
484 (Büning, 1994; de Cuevas et al., 1997; Eastin et al., 2020; Kubrakiewicz, 1997). Given the level
485 of conservation in cell cycle control across species, we propose that Ran and β-importins may also
486 play important roles in higher eukaryotes, connecting the intricate programs of cell division, oocyte
487 differentiation, and cell polarization. This may be of particular consequence for mouse and human
488 oocytes, in which cyst breakdown occurs prior to meiotic onset (Pepling and Lei, 2018).
489 Understanding how Ran and importins control cyst formation and breakdown may help elucidate
490 how the oocyte reserve is established in humans, offering new potential avenues for treatment of
491 infertility.
492

493 **MATERIALS AND METHODS**

494 ***Drosophila strains and husbandry***

495 Flies were maintained at 22°-25°C in standard medium (cornmeal/molasses/yeast/agar)
496 (NutriFly MF; Genesee Scientific). Female progeny were collected one to two days after eclosion
497 and maintained on standard medium for 3, 6, and 10 days at 25°C; flies were fed wet yeast paste
498 for 2-3 days (changed daily) prior to ovary dissection. A complete list of fly lines used in this study
499 are provided in Supp. Table S1.
500

501 ***Tissue-specific RNA interference (RNAi) generation***

502 All RNAi lines used in this study were carried in *pVALIUM20* or *pVALIUM22* transposons
503 for maximum germline efficiency (Supp. Table S1). *UAS-Tnpo-SR*^{V22} was generated as described
504 (www.flyrnai.org/TRiP-HOME.html) (Ni et al., 2011). Primers were designed against the full-
505 length *Tnpo-SR* RNA via the Designer of Small Interfering RNA tool
506 (http://biodev.extra.cea.fr/DSIR/DSIRhtml) using default settings (21 nt siRNA; score threshold
507 90). A sequence with a score of 94.6 and 0 predicted off-targets was selected for hairpin generation
508 (passenger strand, CGATCCCGTTTACTGGATAGA; guide strand,
509 TCTATCCAGTAAACGGGATC). Primers were designed according to TRiP recommendations,
510 annealed to form double-stranded oligos, and ligated into EcoRI-HF/NheI-HF-digested

511 *pVALIUM22*. Transgenic flies (*UAS-Tnpo-SR*^{V22}) were generated by phiC31 site-specific integrase
512 into the *attP2* site on the third chromosome.
513 For RNAi experiments, germline knock-down was facilitated by expressing the germline-
514 specific *nos-GAL4::VP16-nos.UTR* (referred to throughout as *nos-Gal4*) (Rørth, 1998; Van Doren
515 et al., 1998). Driver expression was confirmed using *w*; nos-Gal4, UASp-tubGFP* (BDSC #7253)
516 (Grieder et al., 2000). Females carrying *nos-Gal4* alone were used as controls.
517
518 ***Drosophila genetic mosaic generation***
519 For genetic mosaic analyses using *flippase (FLP)/FLP recognition target (FRT)*, we
520 obtained the following mutant alleles of *FRT*-containing chromosome arms: *Tnpo-SR*^{KG04870}
521 [Kyoto *Drosophila* Stock Center (KDSC) #111581] (Bellen et al., 2004) and *Tnpo-SR*^{LL05552}
522 (KDSC #141628) (Schuldiner et al., 2008). Other genetic tools are described in FlyBase version
523 FB2020_05 (Thurmond et al., 2019). Genetic mosaics were generated by *FLP*/*FRT*-mediated
524 recombination in 2-3-day old females carrying a mutant allele in trans to a wildtype allele (linked
525 to a *Ubi-GFP* marker) on homologous *FRT* arms, and a *hs-FLP* transgene, as described (Laws and
526 Drummond-Barbosa, 2015). Flies were heat shocked at 37°C two times per day for 3 days and
527 incubated at 25°C for 4, 8, or 12 days and supplemented with wet yeast paste on the last 2 days
528 prior to dissection. Wild-type alleles were used for the generation of control (mock) mosaics.
529
530 ***Germ cell analyses***
531 GSCs were identified based on the juxtaposition of their fusomes to the junction with
532 adjacent cap cells (de Cuevas and Spradling, 1998). In *FLP*/*FRT* mutants, GSC loss was measured
533 two ways. First, as the percentage of total mosaic germaria showing evidence of recent stem cell
534 loss; namely, the presence of GFP-negative daughters (cystoblasts/cysts generated from an original
535 GFP-negative stem cell) in the absence of the GFP-negative mother stem cell (Laws and
536 Drummond-Barbosa, 2015). Second, as the percentage of total germaria analyzed that had at least
537 one GFP-negative GSC. All results were subjected to Chi-Square analyses using Microsoft Excel.
538 In RNAi progeny, GSC loss was measured as the average number of GSCs present over three
539 timepoints. Results were subjected to Student's two-tailed T-test comparing driver controls versus
540 *driver>UAS-RNAi* experimental groups at each timepoint individually using Microsoft Excel.

541 For analyses involving the egg chambers outside of the germarium, data was collected from
542 the first three egg chambers posteriorly located from the germarium. Oocytes were identified by
543 the presence of anti-Orb antibodies. The number of cells and ring canals per egg chamber were
544 calculated based on visualization of ring canals with anti-pTyr and/or anti-Hts-RC antibodies and
545 cell nuclei with DAPI. Results were subjected to Student's two-tailed T-test comparing driver
546 controls versus *driver>UAS-RNAi* experimental groups at each timepoint individually using
547 Microsoft Excel and Prism (GraphPad).
548
549 ***Immunofluorescence and microscopy***
550 Ovaries were prepared for immunofluorescence microscopy as described (Grieder et al.,
551 2000; Hinnant et al., 2017). In the standard protocol, ovaries were dissected and teased apart in
552 Grace's medium without additives (Caisson Labs) and fixed in 5.3% formaldehyde in Grace's
553 medium for 13 minutes at room temperature. They were then washed extensively in phosphate-
554 buffered saline (PBS, pH 7.4; Fisher) with 0.1% Triton X-100, and blocked for three hours in
555 blocking solution [5% bovine serum albumin (Sigma), 5% normal goat serum (MP Biomedicals),
556 and 0.1% Triton X-100 in PBS] at room temperature. To detect cells in S phase, dissected ovaries
557 were incubated for one hour at room temperature in Grace's media containing 10 μM 5-ethynyl-
558 2′-deoxyuridine (EdU; Life Technologies). The following primary antibodies were diluted in
559 blocking solution and used overnight at 4°C: chicken anti-GFP (#13970, Abcam; 1:2000), rabbit
560 anti-dsRed (#632496, Clontech; 1:500), rabbit anti-phosphoHistone H3 (pHH3; #06-570,
561 Millipore; 1:200), rat anti-E-Cadherin (DCAD2, Developmental Studies Hybridoma Bank
562 (DSHB); 1:20), mouse anti-Orb (4H8 and 6H4; DSHB; 1:500), mouse anti-BicD (1B11 and 4C2;
563 DSHB; 1:10), mouse anti-p-Tyrosine (Millipore; 1:100), mouse anti-Hts-RC (DSHB; 1:10),
564 mouse anti-CycA (A12; DSHB; 1:50), rabbit anti-C(3)G (a gift from M. Lilly; 1:3000), rat anti-
565 HA (3F10; Sigma; 1:25), mouse anti-α-Tubulin-AF555 (DM1A-AF555; Millipore; 1:100), and
566 rabbit anti-Anillin (a gift from J. Brill; 1:50). Mouse anti-Sxl (m18; DSHB; 1:500) was also used
567 but fixed in a 4% formaldehyde in Grace's medium. Primary antibodies mouse anti-Hts (1B1,
568 DSHB; 1:10), and mouse anti-Lamin C (LC28.26, DSHB; 1:100) were incubated over two nights
569 at 4°C. All primary antibodies are followed by a two hour incubation at room temperature with
570 AlexaFluor 488-, 568- or 633-conjugated goat species-specific secondary antibodies (Life

571 Technologies; 1:200). EdU was detected (if necessary) using AlexaFluor-594 or -647 via Click-
572 It chemistry, following the manufacturer's recommendations (Life Technologies).
573 For stabilizing structures such as mitotic spindles, ovaries were dissected and teased apart
574 in room temperature equilibrated Grace's medium and fixed for 10 minutes at room temperature
575 using 350µl Grace's Medium and 200µl of 16% formaldehyde. They were then extensively washed
576 in PBS with 0.1% Triton X-100 and blocked at room temperature for at least 30 minutes in
577 blocking solution (2.5mL NGS, 5mL Triton, 42.5mL 1xPBS). Primary antibody incubations took
578 place overnight at 4°C followed by extensive washing in PBS with 0.1% Triton X-100 and another
579 blocking period of at least 30 minutes at room temperature. Detection of secondary antibodies
580 proceeded as described above.
581 All ovary samples were stained with 0.5 µg/ml 4'-6-diamidino-2-phenylindole (DAPI;
582 Sigma) in 0.1% Triton X-100 in PBS, and mounted in 90% glycerol mixed with 20% n-propyl
583 gallate (Sigma). Confocal z-stacks (1 µm optical sections) were collected with either the Zeiss
584 LSM700 laser scanning microscope using ZEN Black 2012 software or the Zeiss LSM800 laser
585 scanning microscope using ZEN Blue 2012. Images were analyzed using Zeiss ZEN software, and
586 minimally and equally enhanced via histogram using ZEN and Adobe Photoshop Creative Suite.
587

588 **ACKNOWLEDGMENTS**

589 Many thanks to K. McKim, B. Riggs, K. Roper, J.-Q. Ni, M. Lilly, D. Drummond-Barbosa, M.
590 Buszczak, L. Cooley, and J. Brill for their kind gifts of fly stocks and antibodies. We are grateful
591 to the Bloomington, Vienna, and Kyoto *Drosophila* Stock Centers, the Drosophila Genomics
592 Resource Center, the Harvard Transgenic RNAi Project, and the University of Iowa
593 Developmental Studies Hybridoma Bank for making fly lines, antibodies, and plasmids available,
594 and BestGene for *Drosophila* transgenesis and screening. Many thanks to Tianna Van Cura and
595 members of the Ables laboratory for assistance with building tools, helpful discussions, and critical
596 reading of this manuscript.
597

598 **COMPETING INTERESTS**

599 The authors declare no competing conflicts of interest.
600

601 **FUNDING**

602 This work was supported by National Institutes of Health R15-GM117502 (E. T. A.).

603

604 **DATA AVAILABILITY**

605 Fly strains and plasmids are available upon request. The authors affirm that all data necessary for
606 confirming the conclusions of the article are present within the article and figures.

607

608 **REFERENCES**

609 **Ables, E. T. and Drummond-Barbosa, D.** (2013). Cyclin E controls Drosophila female germline stem cell
610 maintenance independently of its role in proliferation by modulating responsiveness to niche
611 signals. *Development* **140**, 530-540.
612 **Ables, E. T., Hwang, G. H., Finger, D. S., Hinnant, T. D. and Drummond-Barbosa, D.** (2016). A Genetic
613 Mosaic Screen Reveals Ecdysone-Responsive Genes Regulating Drosophila Oogenesis. *G3*
614 *(Bethesda, Md.)* **6**, 2629-2642.
615 **Allemand, E., Dokudovskaya, S., Bordonné, R. and Tazi, J.** (2002). A conserved Drosophila transportin-
616 serine/arginine-rich (SR) protein permits nuclear import of Drosophila SR protein splicing factors
617 and their antagonist repressor splicing factor 1. *Molecular biology of the cell* **13**, 2436-2447.
618 **Ameku, T. and Niwa, R.** (2016). Mating-Induced Increase in Germline Stem Cells via the Neuroendocrine
619 System in Female Drosophila. *PLoS genetics* **12**, e1006123.
620 **Beaudet, D., Akhshi, T., Phillipp, J., Law, C. and Piekny, A.** (2017). Active Ran regulates anillin function
621 during cytokinesis. *Molecular biology of the cell* **28**, 3517-3531.
622 **Beaudet, D., Pham, N., Skaik, N. and Piekny, A.** (2020). Importin binding mediates the intramolecular
623 regulation of anillin during cytokinesis. *Molecular biology of the cell* **31**, 1124-1139.
624 **Bellen, H. J., Levis, R. W., Liao, G., He, Y., Carlson, J. W., Tsang, G., Evans-Holm, M., Hiesinger, P. R.,**
625 **Schulze, K. L., Rubin, G. M., et al.** (2004). The BDGP gene disruption project: single transposon
626 insertions associated with 40% of Drosophila genes. *Genetics* **167**, 761-781.
627 **Bradley, T., Cook, M. E. and Blanchette, M.** (2015). SR proteins control a complex network of RNA-
628 processing events. *Rna* **21**, 75-92.
629 **Büning, J.** (1994). *The Insect Ovary: Ultrastructure, previtellogenic growth and evolution*: Springer,
630 Dordrecht.
631 **Buszczak, M., Paterno, S., Lighthouse, D., Bachman, J., Planck, J., Owen, S., Skora, A. D., Nystul, T. G.,**
632 **Ohlstein, B., Allen, A., et al.** (2007). The carnegie protein trap library: a versatile tool for
633 Drosophila developmental studies. *Genetics* **175**, 1505-1531.
634 **Cautain, B., Hill, R., de Pedro, N. and Link, W.** (2015). Components and regulation of nuclear transport
635 processes. *The FEBS journal* **282**, 445-462.
636 **Cesario, J. and McKim, K. S.** (2011). RanGTP is required for meiotic spindle organization and the
637 initiation of embryonic development in Drosophila. *J Cell Sci* **124**, 3797-3810.
638 **Chaigne, A., Labouesse, C., White, I. J., Agnew, M., Hannezo, E., Chalut, K. J. and Paluch, E. K.** (2020).
639 Abscission Couples Cell Division to Embryonic Stem Cell Fate. *Developmental cell* **55**, 195-
640 208.e195.
641 **Chau, J., Kulnane, L. S. and Salz, H. K.** (2009). Sex-lethal facilitates the transition from germline stem cell
642 to committed daughter cell in the Drosophila ovary. *Genetics* **182**, 121-132.
643 **Chen, A., Akhshi, T. K., Lavoie, B. D. and Wilde, A.** (2015). Importin β2 Mediates the Spatio-temporal
644 Regulation of Anillin through a Noncanonical Nuclear Localization Signal. *The Journal of*
645 *biological chemistry* **290**, 13500-13509.

646 **Chen, D., Wang, Q., Huang, H., Xia, L., Jiang, X., Kan, L., Sun, Q. and Chen, D.** (2009). Effete-mediated
647 degradation of Cyclin A is essential for the maintenance of germline stem cells in Drosophila.
648 *Development* **136**, 4133-4142.
649 **Chen, J., Call, G. B., Beyer, E., Bui, C., Cespedes, A., Chan, A., Chan, J., Chan, S., Chhabra, A., Dang, P.,**
650 **et al.** (2005). Discovery-based science education: functional genomic dissection in Drosophila by
651 undergraduate researchers. *PLoS Biol* **3**, e59.
652 **Cheng, J., Türkel, N., Hemati, N., Fuller, M. T., Hunt, A. J. and Yamashita, Y. M.** (2008). Centrosome
653 misorientation reduces stem cell division during ageing. *Nature* **456**, 599-604.
654 **de Cuevas, M., Lee, J. K. and Spradling, A. C.** (1996). alpha-spectrin is required for germline cell division
655 and differentiation in the Drosophila ovary. *Development* **122**, 3959-3968.
656 **de Cuevas, M., Lilly, M. A. and Spradling, A. C.** (1997). Germline cyst formation in Drosophila. *Annual*
657 *review of genetics* **31**, 405-428.
658 **de Cuevas, M. and Spradling, A. C.** (1998). Morphogenesis of the Drosophila fusome and its implications
659 for oocyte specification. *Development* **125**, 2781-2789.
660 **Deng, W. and Lin, H.** (1997). Spectrosomes and fusomes anchor mitotic spindles during asymmetric
661 germ cell divisions and facilitate the formation of a polarized microtubule array for oocyte
662 specification in Drosophila. *Developmental biology* **189**, 79-94.
663 **Drutovic, D., Duan, X., Li, R., Kalab, P. and Solc, P.** (2020). RanGTP and importin β regulate meiosis I
664 spindle assembly and function in mouse oocytes. *The EMBO journal* **39**, e101689.
665 **Eastin, K. J., Huang, A. P. and Ferree, P. M.** (2020). A novel pattern of germ cell divisions in the
666 production of hymenopteran insect eggs. *Biol Lett* **16**, 20200137.
667 **Eikenes Å, H., Malerød, L., Lie-Jensen, A., Sem Wegner, C., Brech, A., Liestøl, K., Stenmark, H. and**
668 **Haglund, K.** (2015). Src64 controls a novel actin network required for proper ring canal
669 formation in the Drosophila male germline. *Development* **142**, 4107-4118.
670 **Fichelson, P., Jagut, M., Lepanse, S., Lepesant, J. A. and Huynh, J. R.** (2010). lethal giant larvae is
671 required with the par genes for the early polarization of the Drosophila oocyte. *Development*
672 **137**, 815-824.
673 **Forbes, D. J., Travesa, A., Nord, M. S. and Bernis, C.** (2015). Nuclear transport factors: global regulation
674 of mitosis. *Current opinion in cell biology* **35**, 78-90.
675 **Frémont, S. and Echard, A.** (2018). Membrane Traffic in the Late Steps of Cytokinesis. *Current biology :*
676 *CB* **28**, R458-R470.
677 **Geles, K. G. and Adam, S. A.** (2001). Germline and developmental roles of the nuclear transport factor
678 importin alpha3 in C. elegans. *Development* **128**, 1817-1830.
679 **Goldbach, P., Wong, R., Beise, N., Sarpal, R., Trimble, W. S. and Brill, J. A.** (2010). Stabilization of the
680 actomyosin ring enables spermatocyte cytokinesis in Drosophila. *Molecular biology of the cell*
681 **21**, 1482-1493.
682 **Grieder, N. C., de Cuevas, M. and Spradling, A. C.** (2000). The fusome organizes the microtubule
683 network during oocyte differentiation in Drosophila. *Development* **127**, 4253-4264.
684 **Guertin, D. A., Trautmann, S. and McCollum, D.** (2002). Cytokinesis in eukaryotes. *Microbiology and*
685 *molecular biology reviews : MMBR* **66**, 155-178.
686 **Haglund, K., Nezis, I. P., Lemus, D., Grabbe, C., Wesche, J., Liestøl, K., Dikic, I., Palmer, R. and**
687 **Stenmark, H.** (2010). Cindr interacts with anillin to control cytokinesis in Drosophila
688 melanogaster. *Current biology : CB* **20**, 944-950.
689 **Haglund, K., Nezis, I. P. and Stenmark, H.** (2011). Structure and functions of stable intercellular bridges
690 formed by incomplete cytokinesis during development. *Communicative & integrative biology* **4**,
691 1-9.
692 **Hinnant, T. D., Alvarez, A. A. and Ables, E. T.** (2017). Temporal remodeling of the cell cycle accompanies
693 differentiation in the Drosophila germline. *Developmental biology* **429**, 118-131.

694 **Hinnant, T. D., Merkle, J. A. and Ables, E. T.** (2020). Coordinating Proliferation, Polarity, and Cell Fate in
695 the Drosophila Female Germline. *Frontiers in cell and developmental biology* **8**, 19.
696 **Hogarth, C., Itman, C., Jans, D. A. and Loveland, K. L.** (2005). Regulated nucleocytoplasmic transport in
697 spermatogenesis: a driver of cellular differentiation? *BioEssays : news and reviews in molecular,*
698 *cellular and developmental biology* **27**, 1011-1025.
699 **Hughes, S. E., Miller, D. E., Miller, A. L. and Hawley, R. S.** (2018). Female Meiosis: Synapsis,
700 Recombination, and Segregation in Drosophila melanogaster. *Genetics* **208**, 875-908.
701 **Huynh, J.-R.** (2006). Fusome as a Cell-Cell Communication Channel of Drosophila Ovarian Cyst. In *Cell-*
702 *Cell Channels* (ed. F. Baluska, D. Volkmann & P. W. Barlow), pp. 217-235. New York, NY: Springer
703 New York.
704 **Ji, S., Li, C., Hu, L., Liu, K., Mei, J., Luo, Y., Tao, Y., Xia, Z., Sun, Q. and Chen, D.** (2017). Bam-dependent
705 deubiquitinase complex can disrupt germ-line stem cell maintenance by targeting cyclin A.
706 *Proceedings of the National Academy of Sciences of the United States of America* **114**, 6316-
707 6321.
708 **Kimura, M. and Imamoto, N.** (2014). Biological significance of the importin-β family-dependent
709 nucleocytoplasmic transport pathways. *Traffic (Copenhagen, Denmark)* **15**, 727-748.
710 **Kimura, M., Morinaka, Y., Imai, K., Kose, S., Horton, P. and Imamoto, N.** (2017). Extensive cargo
711 identification reveals distinct biological roles of the 12 importin pathways. *eLife* **6**.
712 **King, R. C. R. C.** (1970). Ovarian development in Drosophila melanogaster. New York: Academic Press.
713 **Koch, E. A. and King, R. C.** (1966). The origin and early differentiation of the egg chamber of Drosophila
714 melanogaster. *J Morphol* **119**, 283-303.
715 **Koch, E. A., Smith, P. A. and King, R. C.** (1967). The division and differentiation of Drosophila cystocytes.
716 *J Morphol* **121**, 55-70.
717 **Kubrakiewicz, J.** (1997). Germ cells cluster organization in polytrophic ovaries of neuroptera. *Tissue and*
718 *Cell* **29**, 221-228.
719 **Lai, M. C., Lin, R. I. and Tarn, W. Y.** (2001). Transportin-SR2 mediates nuclear import of phosphorylated
720 SR proteins. *Proc Natl Acad Sci U S A* **98**, 10154-10159.
721 **Laws, K. M. and Drummond-Barbosa, D.** (2015). Genetic Mosaic Analysis of Stem Cell Lineages in the
722 Drosophila Ovary. *Methods in molecular biology (Clifton, N.J.)* **1328**, 57-72.
723 **Lighthouse, D. V., Buszczak, M. and Spradling, A. C.** (2008). New components of the Drosophila fusome
724 suggest it plays novel roles in signaling and transport. *Developmental biology* **317**, 59-71.
725 **Lilly, M. A., de Cuevas, M. and Spradling, A. C.** (2000). Cyclin A associates with the fusome during
726 germline cyst formation in the Drosophila ovary. *Developmental biology* **218**, 53-63.
727 **Lin, H. and Spradling, A. C.** (1995). Fusome asymmetry and oocyte determination in Drosophila. *Dev*
728 *Genet* **16**, 6-12.
729 **Lin, H., Yue, L. and Spradling, A. C.** (1994). The Drosophila fusome, a germline-specific organelle,
730 contains membrane skeletal proteins and functions in cyst formation. *Development* **120**, 947-
731 956.
732 **Lippai, M., Tirián, L., Boros, I., Mihály, J., Erdélyi, M., Belecz, I., Máthé, E., Pósfai, J., Nagy, A., Udvardy,**
733 **A., et al.** (2000). The Ketel gene encodes a Drosophila homologue of importin-beta. *Genetics*
734 **156**, 1889-1900.
735 **Loveland, K. L., Major, A. T., Butler, R., Young, J. C., Jans, D. A. and Miyamoto, Y.** (2015). Putting things
736 in place for fertilization: discovering roles for importin proteins in cell fate and spermatogenesis.
737 *Asian journal of andrology* **17**, 537-544.
738 **Lu, K., Jensen, L., Lei, L. and Yamashita, Y. M.** (2017). Stay Connected: A Germ Cell Strategy. *Trends in*
739 *genetics : TIG* **33**, 971-978.

Maertens, G. N., Cook, N. J., Wang, W., Hare, S., Gupta, S. S., Öztop, I., Lee, K., Pye, V. E., Cosnefroy, O., Snijders, A. P., et al. (2014). Structural basis for nuclear import of splicing factors by human Transportin 3. *Proc Natl Acad Sci U S A* **111**, 2728-2733.

Mahowald, A. P. (1971). The formation of ring canals by cell furrows in Drosophila. *Z Zellforsch Mikrosk Anat* **118**, 162-167.

Mason, D. A., Fleming, R. J. and Goldfarb, D. S. (2002). Drosophila melanogaster importin alpha1 and alpha3 can replace importin alpha2 during spermatogenesis but not oogenesis. *Genetics* **161**, 157-170.

Máthé, E., Bates, H., Huikeshoven, H., Deák, P., Glover, D. M. and Cotterill, S. (2000). Importin-alpha3 is required at multiple stages of Drosophila development and has a role in the completion of oogenesis. *Developmental biology* **223**, 307-322.

Máthé, E., Inoue, Y. H., Palframan, W., Brown, G. and Glover, D. M. (2003). Orbit/Mast, the CLASP orthologue of Drosophila, is required for asymmetric stem cell and cystocyte divisions and development of the polarised microtubule network that interconnects oocyte and nurse cells during oogenesis. *Development* **130**, 901-915.

Mathieu, J., Cauvin, C., Moch, C., Radford, S. J., Sampaio, P., Perdigoto, C. N., Schweisguth, F., Bardin, A. J., Sunkel, C. E., McKim, K., et al. (2013). Aurora B and cyclin B have opposite effects on the timing of cytokinesis abscission in Drosophila germ cells and in vertebrate somatic cells. *Developmental cell* **26**, 250-265.

Mathieu, J. and Huynh, J. R. (2017). Monitoring complete and incomplete abscission in the germ line stem cell lineage of Drosophila ovaries. *Methods in cell biology* **137**, 105-118.

Matias, N. R., Mathieu, J. and Huynh, J. R. (2015). Abscission is regulated by the ESCRT-III protein shrub in Drosophila germline stem cells. *PLoS genetics* **11**, e1004653.

Matova, N. and Cooley, L. (2001). Comparative aspects of animal oogenesis. *Developmental biology* **231**, 291-320.

McKearin, D. (1997). The Drosophila fusome, organelle biogenesis and germ cell differentiation: if you build it. *BioEssays : news and reviews in molecular, cellular and developmental biology* **19**, 147-152.

McKearin, D. and Ohlstein, B. (1995). A role for the Drosophila bag-of-marbles protein in the differentiation of cystoblasts from germline stem cells. *Development* **121**, 2937-2947.

Megraw, T. L. and Kaufman, T. C. (2000). The centrosome in Drosophila oocyte development. *Current topics in developmental biology* **49**, 385-407.

Mihalas, B. P., Western, P. S., Loveland, K. L., McLaughlin, E. A. and Holt, J. E. (2015). Changing expression and subcellular distribution of karyopherins during murine oogenesis. *Reproduction (Cambridge, England)* **150**, 485-496.

Morris, J. Z., Hong, A., Lilly, M. A. and Lehmann, R. (2005). twin, a CCR4 homolog, regulates cyclin poly(A) tail length to permit Drosophila oogenesis. *Development* **132**, 1165-1174.

Nguyen, L. T. S. and Robinson, D. N. (2020). The Unusual Suspects in Cytokinesis: Fitting the Pieces Together. *Frontiers in cell and developmental biology* **8**, 441.

Ni, J. Q., Zhou, R., Czech, B., Liu, L. P., Holderbaum, L., Yang-Zhou, D., Shim, H. S., Tao, R., Handler, D., Karpowicz, P., et al. (2011). A genome-scale shRNA resource for transgenic RNAi in Drosophila. *Nat Methods* **8**, 405-407.

Ohlmeyer, J. T. and Schüpbach, T. (2003). Encore facilitates SCF-Ubiquitin-proteasome-dependent proteolysis during Drosophila oogenesis. *Development* **130**, 6339-6349.

Okada, N., Ishigami, Y., Suzuki, T., Kaneko, A., Yasui, K., Fukutomi, R. and Isemura, M. (2008). Importins and exportins in cellular differentiation. *J Cell Mol Med* **12**, 1863-1871.

Ong, S. and Tan, C. (2010). Germline cyst formation and incomplete cytokinesis during Drosophila melanogaster oogenesis. *Developmental biology* **337**, 84-98.

788 **Ozugergin, I. and Piekny, A.** (2020). Complementary functions for the Ran gradient during division.
789 *Small GTPases*, 1-11.
790 **Pepling, M. and Lei, L.** (2018). Germ Cell Nests and Germline Cysts. In *Encyclopedia of Reproduction*
791 *(Second Edition)* (ed. M. K. Skinner), pp. 159-166. Oxford: Academic Press.
792 **Pepling, M. E., de Cuevas, M. and Spradling, A. C.** (1999). Germline cysts: a conserved phase of germ
793 cell development? *Trends in Cell Biology* **9**, 257-262.
794 **Perkins, L. A., Holderbaum, L., Tao, R., Hu, Y., Sopko, R., McCall, K., Yang-Zhou, D., Flockhart, I., Binari,**
795 **R., Shim, H. S., et al.** (2015). The Transgenic RNAi Project at Harvard Medical School: Resources
796 and Validation. *Genetics* **201**, 843-852.
797 **Petrella, L. N., Smith-Leiker, T. and Cooley, L.** (2007). The Ovhts polyprotein is cleaved to produce
798 fusome and ring canal proteins required for Drosophila oogenesis. *Development* **134**, 703-712.
799 **Piekny, A. J. and Maddox, A. S.** (2010). The myriad roles of Anillin during cytokinesis. *Seminars in cell &*
800 *developmental biology* **21**, 881-891.
801 **Pollard, T. D. and O'Shaughnessy, B.** (2019). Molecular Mechanism of Cytokinesis. *Annu Rev Biochem*
802 **88**, 661-689.
803 **Robinson, D. N., Cant, K. and Cooley, L.** (1994). Morphogenesis of Drosophila ovarian ring canals.
804 *Development* **120**, 2015-2025.
805 **Röper, K.** (2007). Rtnl1 is enriched in a specialized germline ER that associates with ribonucleoprotein
806 granule components. *J Cell Sci* **120**, 1081-1092.
807 **Rørth, P.** (1998). Gal4 in the Drosophila female germline. *Mech Dev* **78**, 113-118.
808 **Sazer, S. and Dasso, M.** (2000). The ran decathlon: multiple roles of Ran. *J Cell Sci* **113 (Pt 7)**, 1111-1118.
809 **Schuldiner, O., Berdnik, D., Levy, J. M., Wu, J. S., Luginbuhl, D., Gontang, A. C. and Luo, L.** (2008).
810 piggyBac-based mosaic screen identifies a postmitotic function for cohesin in regulating
811 developmental axon pruning. *Developmental cell* **14**, 227-238.
812 **Silverman-Gavrila, R. V., Hales, K. G. and Wilde, A.** (2008). Anillin-mediated targeting of peanut to
813 pseudocleavage furrows is regulated by the GTPase Ran. *Molecular biology of the cell* **19**, 3735-
814 3744.
815 **Snapp, E. L., Iida, T., Frescas, D., Lippincott-Schwartz, J. and Lilly, M. A.** (2004). The fusome mediates
816 intercellular endoplasmic reticulum connectivity in Drosophila ovarian cysts. *Molecular biology*
817 *of the cell* **15**, 4512-4521.
818 **Storto, P. D. and King, R. C.** (1989). The role of polyfusomes in generating branched chains of cystocytes
819 during Drosophila oogenesis. *Dev Genet* **10**, 70-86.
820 **Sugimura, I. and Lilly, M. A.** (2006). Bruno inhibits the expression of mitotic cyclins during the prophase
821 I meiotic arrest of Drosophila oocytes. *Developmental cell* **10**, 127-135.
822 **Teixeira, F. K. and Lehmann, R.** (2019). Translational Control during Developmental Transitions. *Cold*
823 *Spring Harb Perspect Biol* **11**.
824 **Thurmond, J., Goodman, J. L., Strelets, V. B., Attrill, H., Gramates, L. S., Marygold, S. J., Matthews, B.**
825 **B., Millburn, G., Antonazzo, G., Trovisco, V., et al.** (2019). FlyBase 2.0: the next generation.
826 *Nucleic Acids Res* **47**, D759-d765.
827 **Tirián, L., Puro, J., Erdélyi, M., Boros, I., Papp, B., Lippai, M. and Szabad, J.** (2000). The Ketel(D)
828 dominant-negative mutations identify maternal function of the Drosophila importin-beta gene
829 required for cleavage nuclei formation. *Genetics* **156**, 1901-1912.
830 **Trieselmann, N. and Wilde, A.** (2002). Ran localizes around the microtubule spindle in vivo during
831 mitosis in Drosophila embryos. *Current biology : CB* **12**, 1124-1129.
832 **Van Doren, M., Williamson, A. L. and Lehmann, R.** (1998). Regulation of zygotic gene expression in
833 Drosophila primordial germ cells. *Current biology : CB* **8**, 243-246.

Villányi, Z., Debec, A., Timinszky, G., Tirián, L. and Szabad, J. (2008). Long persistence of importin-beta explains extended survival of cells and zygotes that lack the encoding gene. *Mech Dev* **125**, 196-206.

Xu, T. and Rubin, G. M. (1993). Analysis of genetic mosaics in developing and adult Drosophila tissues. *Development* **117**, 1223-1237.

Yamashita, Y. M. (2018). Subcellular Specialization and Organelle Behavior in Germ Cells. *Genetics* **208**, 19-51.

Yue, L. and Spradling, A. C. (1992). hu-li tai shao, a gene required for ring canal formation during Drosophila oogenesis, encodes a homolog of adducin. *Genes & development* **6**, 2443-2454.

Zielke, N., Korzelius, J., van Straaten, M., Bender, K., Schuhknecht, G. F. P., Dutta, D., Xiang, J. and Edgar, B. A. (2014). Fly-FUCCI: A versatile tool for studying cell proliferation in complex tissues. *Cell Rep* **7**, 588-598.

848 **TABLES**

849 **Table 1. Frequency of ovarioles or egg chambers that showcase germline phenotypes in β-**
850 **importin- and Ran-depleted ovaries.**

genotype	% of agametic ovarioles	average # of GSCs at 3 days after eclosion[a]	% of egg chambers that do not equal 16 cells	% of egg chambers that do not equal 2^n germ cells	% of 16-cell egg chambers without an oocyte
driver control	0	2.8	0.64	0	0
Fs(2)Ket^{GL01273}	3.6	1.8 ***	3.9	1.3	0
Ran^{GL01341}	1.5	1.1 ***	11.31***	2.6	4.0
cdm^{HMS02846}	33.1	0.27 ***	32.0 ***	55.0	0
Tnpo-SR^{V22}	2.5	1.5 ***	46.0 ***	29.3	33.8
Ran$^{HA.1}$	0	2.9	0	0	0
Ran$^{HA.2}$	0	2.4	0	0	0
Ran $^{T24N.1}$	63.8	0.25 ***	15.6 ***	12.5	23.5
Ran $^{T24N.2}$	49.6	0.38 ***	19.5***	9.7	11.5
Ran $^{Q69L.1}$	0	1.9 ***	0	0	0
Ran $^{Q69L.2}$	2.0	2.0 ***	6.4 **	2.2	0

851 [a]See Suppl. Figure S1.

852 $^{**}p < 0.01$, $^{***}p < 0.001$. Students two-tailed t-test and Chi-squared test.

853 **FIGURES**

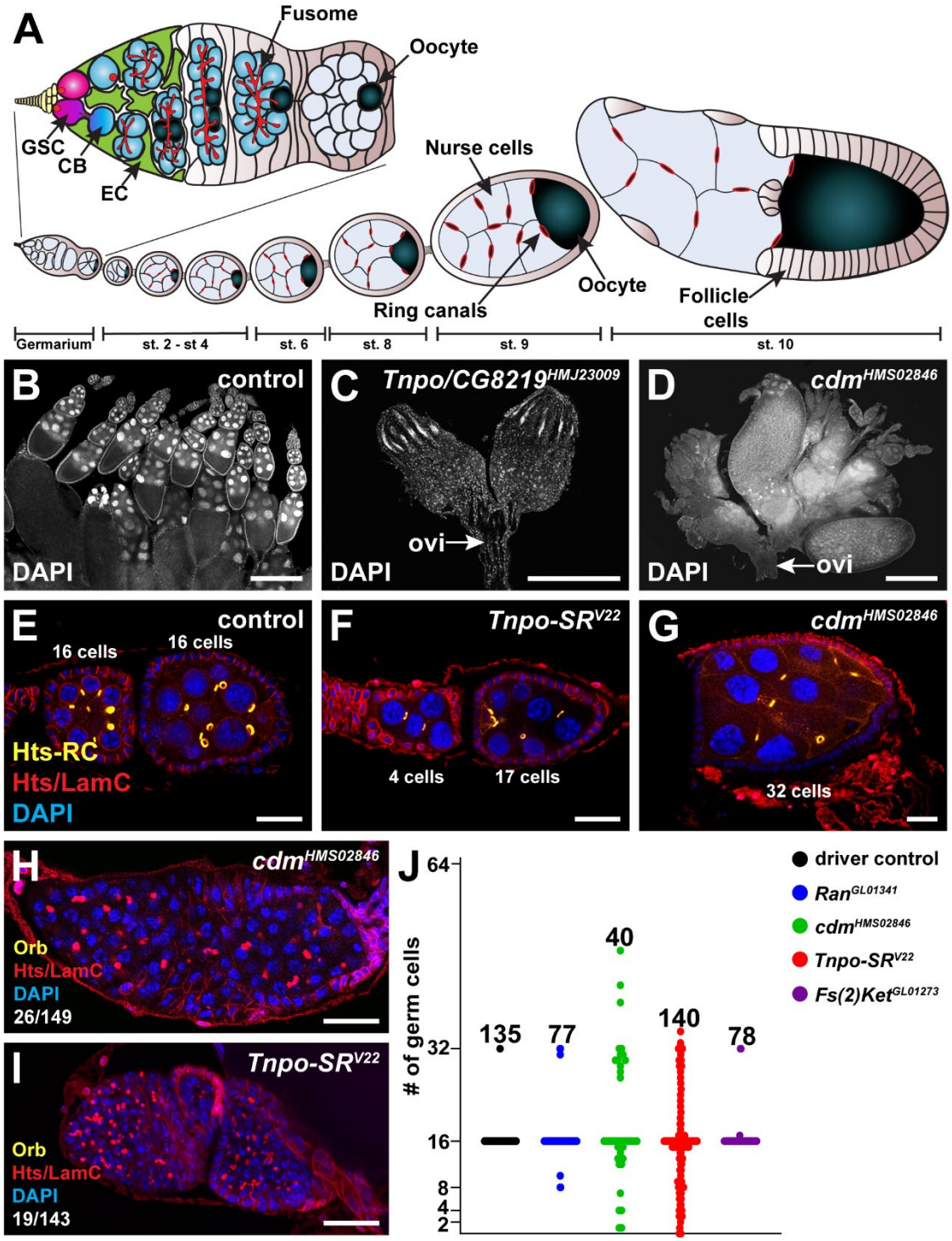

854

855 **Figure 1. An RNAi screen identified Ran and β-importins necessary for germ cell**
856 **development.**

857 (A) The *Drosophila* ovary is composed of ovarioles harboring a germarium (top) and older egg
858 chambers containing developing oocytes (bottom). In the germarium, germline stem cells (GSCs;
859 pink) are adjacent to cap cells (yellow) and escort cells (green). GSCs divide to form cystoblasts
860 (blue) that divide four times to form 16-cell cysts (blue). Cysts are composed of 15 nurse cells and
861 one oocyte (dark blue), connected by 15 intercellular bridges that can be visualized by ring canals
862 and the fusome (red) that transects each bridge. (B-D) Maximum intensity projections of *nos-Gal4*
863 control (B), *nos-Gal4>Tnpo/CG8219*^{HMJ23009} (C), or *nos-Gal4>cdm*^{HMS02846} (D) knockdown
864 ovaries labeled with DAPI (white; nuclei). Arrows indicate oviducts (ovi). Scale bar, 200 µm. (E-
865 G) Egg chambers of driver control (E), *nos-Gal4>Tnpo-SR*^{V22} (F), and *nos-Gal4>cdm*^{HMS02846} (G)
866 ovarioles labeled with anti-Hts-RC (yellow), anti-Hts (red), anti-LamC (red), and DAPI (blue).
867 (H-I) *nos-Gal4>Tnpo-SR*^{V22} (H) and *nos-Gal4>cdm*^{HMS02846} (I) females labeled with anti-Orb
868 (yellow; oocyte), anti-Hts and anti-LamC (red), and DAPI (blue). Values in bottom left corner of
869 G-H represent the number of ovarioles containing germline tumors over the total number of
870 ovarioles analyzed. Scale bar, 20 µm. (J) Number of germ cells per egg chamber at 6 days after
871 eclosion. Each dot represents one egg chamber; numbers above dots represent the total number of
872 egg chambers analyzed. Quantifications do not include tumorous egg chambers.

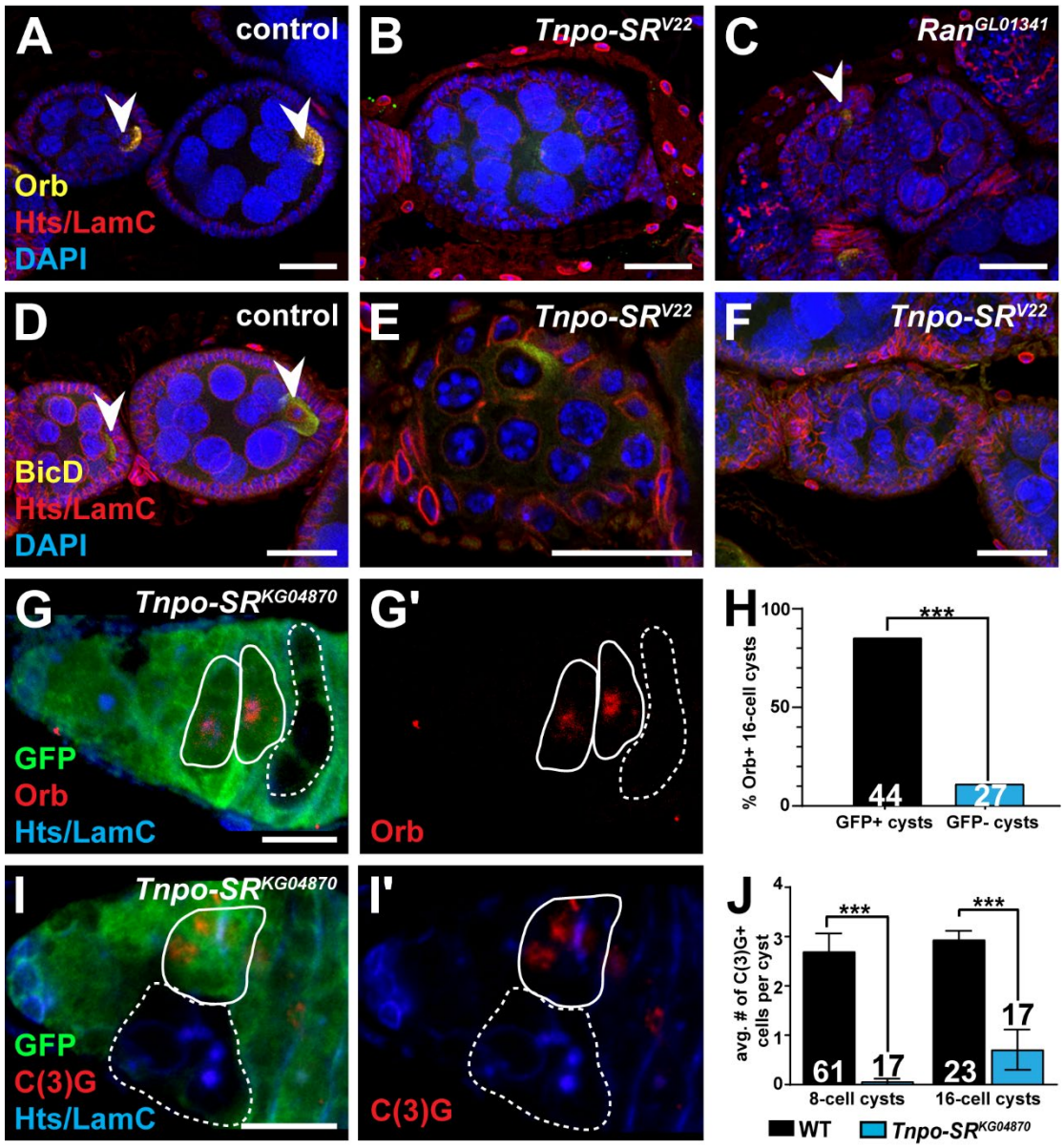

Figure 2. *Ran* and *Tnpo-SR* are required for proper oocyte selection.

(A-C) Driver control (A), *nos-Gal4>Tnpo-SR*^{V22} (B), and *nos-Gal4>Ran*^{GL01341} egg chambers labeled with anti-Orb (yellow), anti-Hts (red), anti-LamC (red), and DAPI (blue). (D-F) Driver control (D) and *nos-Gal4>Tnpo-SR*^{V22} (E-F) egg chambers labeled with anti-BicD (yellow), anti-Hts (red), anti-LamC (red), and DAPI (blue). Arrowheads indicate oocytes, recognized by their condensed nuclei. (G) Frequencies of egg chambers containing 0 (grey), 1 (white), or 2 (black) oocytes. The numbers in the bars represent the total number of egg chambers analyzed. (H-J) *Tnpo-SR*^{KG04870} mutant mosaic germarium at 8 days after clone induction labeled with anti-GFP (green;

882 wild-type cells), anti-Hts and anti-LamC (blue), and anti-Orb (red) (H-H') or anti-C(3)G (red). (J-
883 J'). White lines demarcate wild-type (solid) or mutant (dashed) cysts. (I) Percentage of GFP-
884 positive (wild-type) or GFP-negative (*Tnpo-SR*^{KG04870}) 16-cell cysts with an Orb-positive oocyte
885 8 days after clone induction. (K) Average number of C(3)G-positive germ cells in GFP-positive
886 (wild-type) or GFP-negative (*Tnpo-SR*^{KG04870}) 8- or 16-cell cysts at 8 days after clone induction.
887 Numbers in the bars represent the total number of cysts analyzed. Scale bar, 20 μm (A-F) and 5
888 μm (H-J). Error bars, mean ± SEM. ***$p < 0.001$; Student's two-tailed T-test.

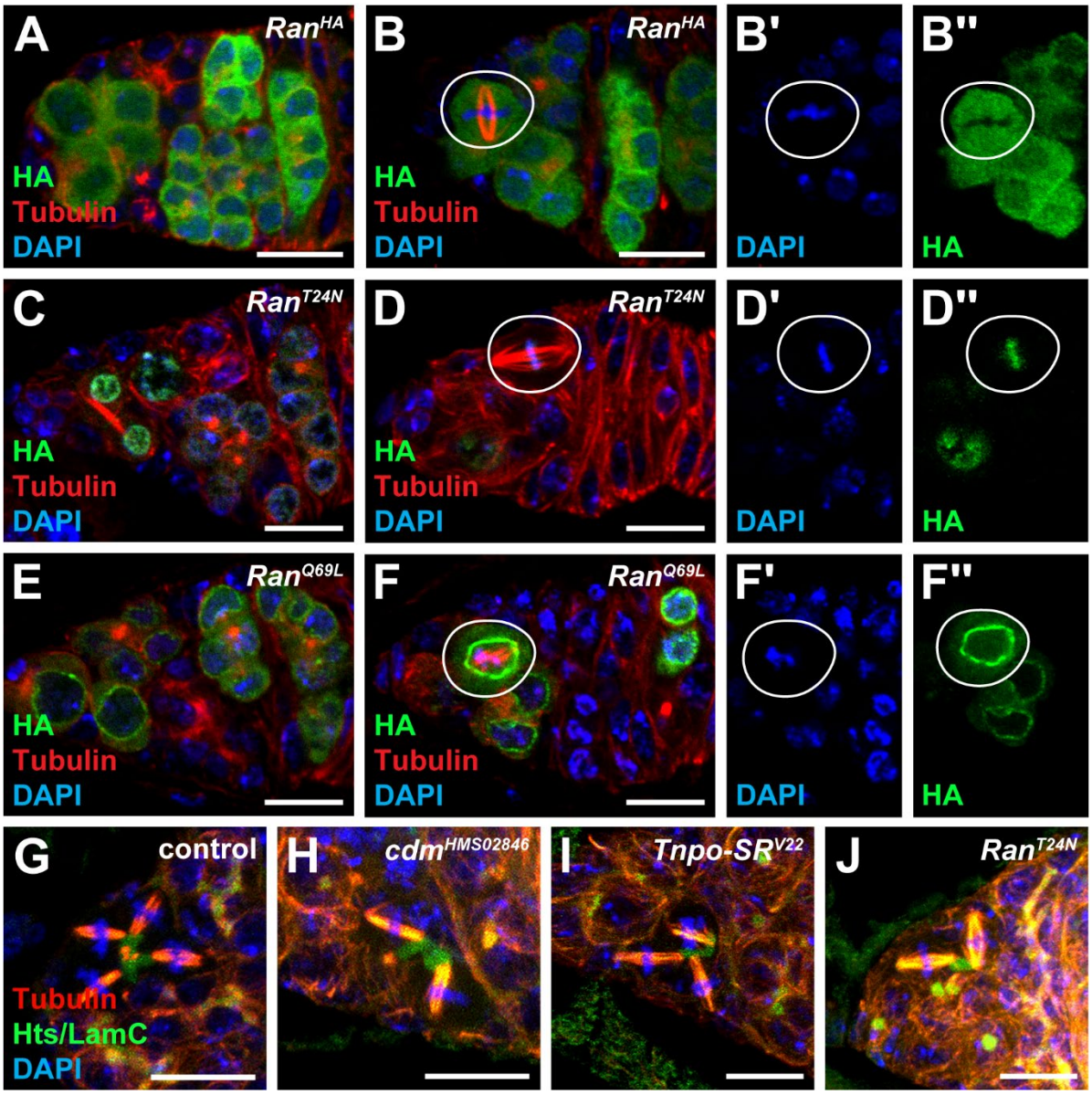

Figure 3. Ran is dynamically localized in germ cells but dispensable for spindle assembly.

(A-F'') Ovarioles from *nos-Gal4>Ran*^{HA} (A-B''), *nos-Gal4>Ran*^{T24N} (C-D''), and *nos-Gal4>Ran*^{Q69L} (E-F'') labeled with anti-HA (green), anti-Tubulin (red) and DAPI (blue). Panels B'-B'', D'-D'', and F'-F'' show the DAPI and HA channels of panels B, D, and F, respectively. (G-J) Maximum intensity projections of driver control (G), RNAi-depleted *cdm*^{HMS02846} (H) and *Tnpo-SR*^{V22} (I), and *Ran*^{T24N} mutant (J) cysts labeled with anti-tubulin (red) anti-Hts (green), anti-LamC (green), and DAPI (blue). Scale bars, 10 µm.

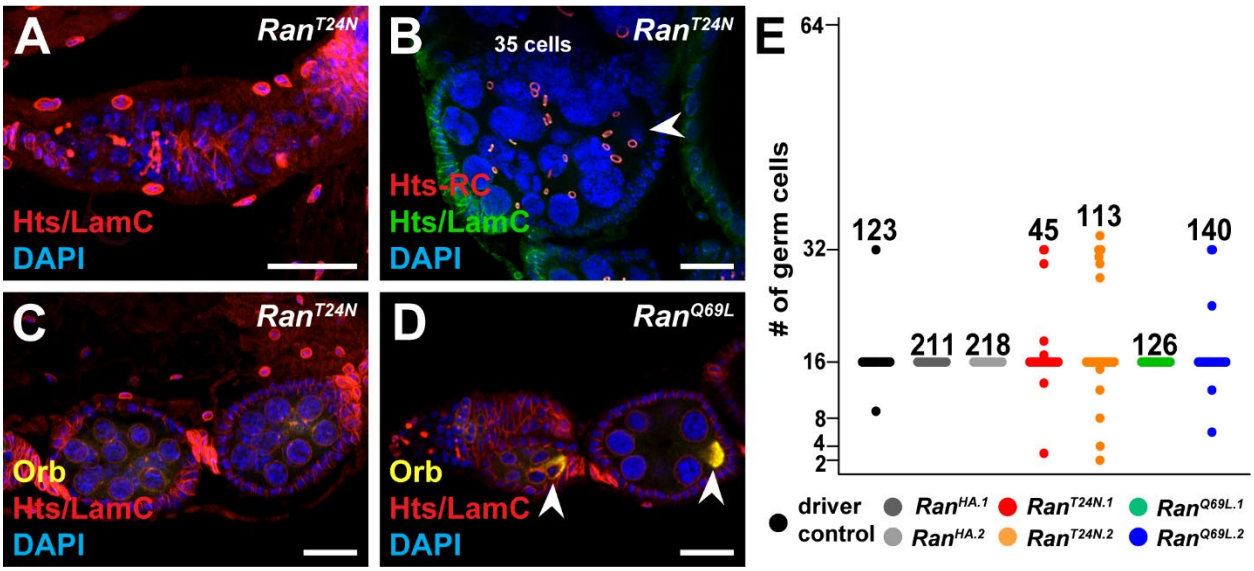

Figure 4. Ran function in dividing germ cells requires Ran-GTP activity.

(A) Maximum intensity projection of a germarium from a *nos-Gal4>Ran*^{T24N} ovary immunostained with anti-Hts (red), anti-LamC (red), and DAPI (blue). (B) Maximum intensity projection of a *Ran*^{T24N} germarium stained with anti-Hts-RC (red), anti-Hts (green), anti-LamC (green), and DAPI (blue). (C-D) *Ran*^{T24N} (C, GDP-locked mutant) and *Ran*^{Q69L} (D, GTP-locked mutant) germaria labeled with anti-Orb (yellow), anti-Hts (red), anti-LamC (red), and DAPI (blue). Arrowheads indicate oocytes, as recognized by their condensed nuclei. Scale bars, 20 µm. (E) Number of germ cells per egg chamber at 6 days after eclosion. Each dot represents one egg chamber; numbers above dots represent the total number of egg chambers analyzed.

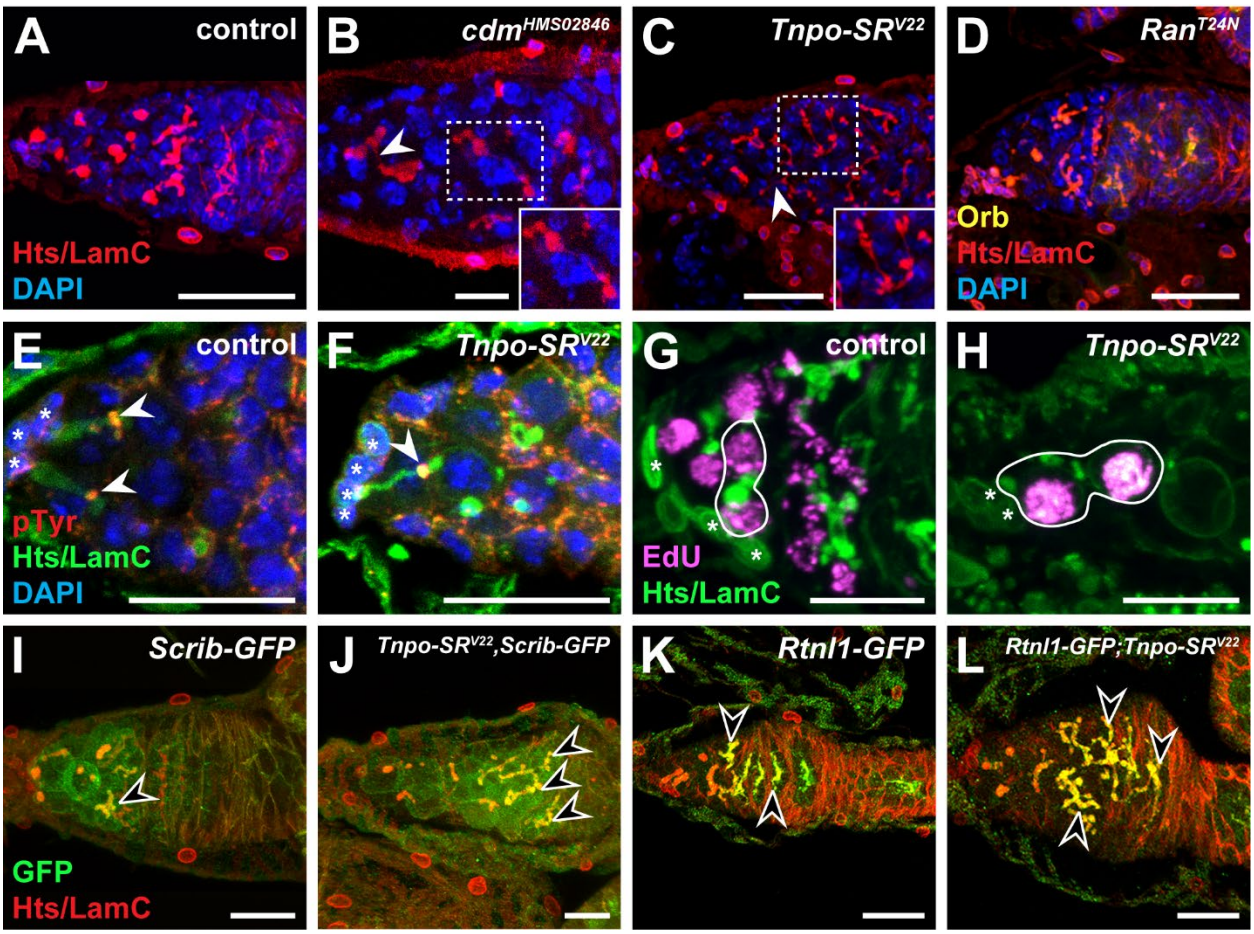

Figure 5. *Tnpo-SR* and *cdm* are required for fusome integrity and maturation.

(A-D) Driver control (A), *cdm*^{HMS02846} (B), *Tnpo-SR*^{V22} (C), and *Ran*^{T24N} (D) germaria labeled with anti-Hts (red), anti-LamC (red), and DAPI (blue). Arrowheads indicate points of the fusome that are thinner than normal. (E-F) Driver control (E) and *nos-Gal4>Tnpo-SR*^{V22} (F) GSC/CB pairs labeled with anti-pTyrosine (red), anti-Hts (green), anti-LamC (green), and DAPI (blue). Arrowheads indicate pTyr+ plug that forms between the GSC/CB pair prior to abscission. (G-H) Control (G) and *nos-Gal4>Tnpo-SR*^{V22} (H) GSC/CB pairs labeled with anti-EdU (magenta), anti-Hts (green) and anti-LamC (green). (I-J) *Scrib-GFP* control (I) and *Tnpo-SR*^{V22}*;Scrib-GFP* (J) germaria labeled with anti-GFP (green), anti-Hts (red), and anti-LamC (red). (K-L) *Rtnl1-GFP* control (K) and *Tnpo-SR*^{V22}*,Rtnl1-GFP* (L) germaria labeled with anti-GFP (green), anti-Hts (red), and anti-LamC (red). Arrowheads indicate highest level of expression of the Scrib (I-J) and Rtnl1 (K-L). All images are maximum intensity projections. Scale bars, 10 µm.

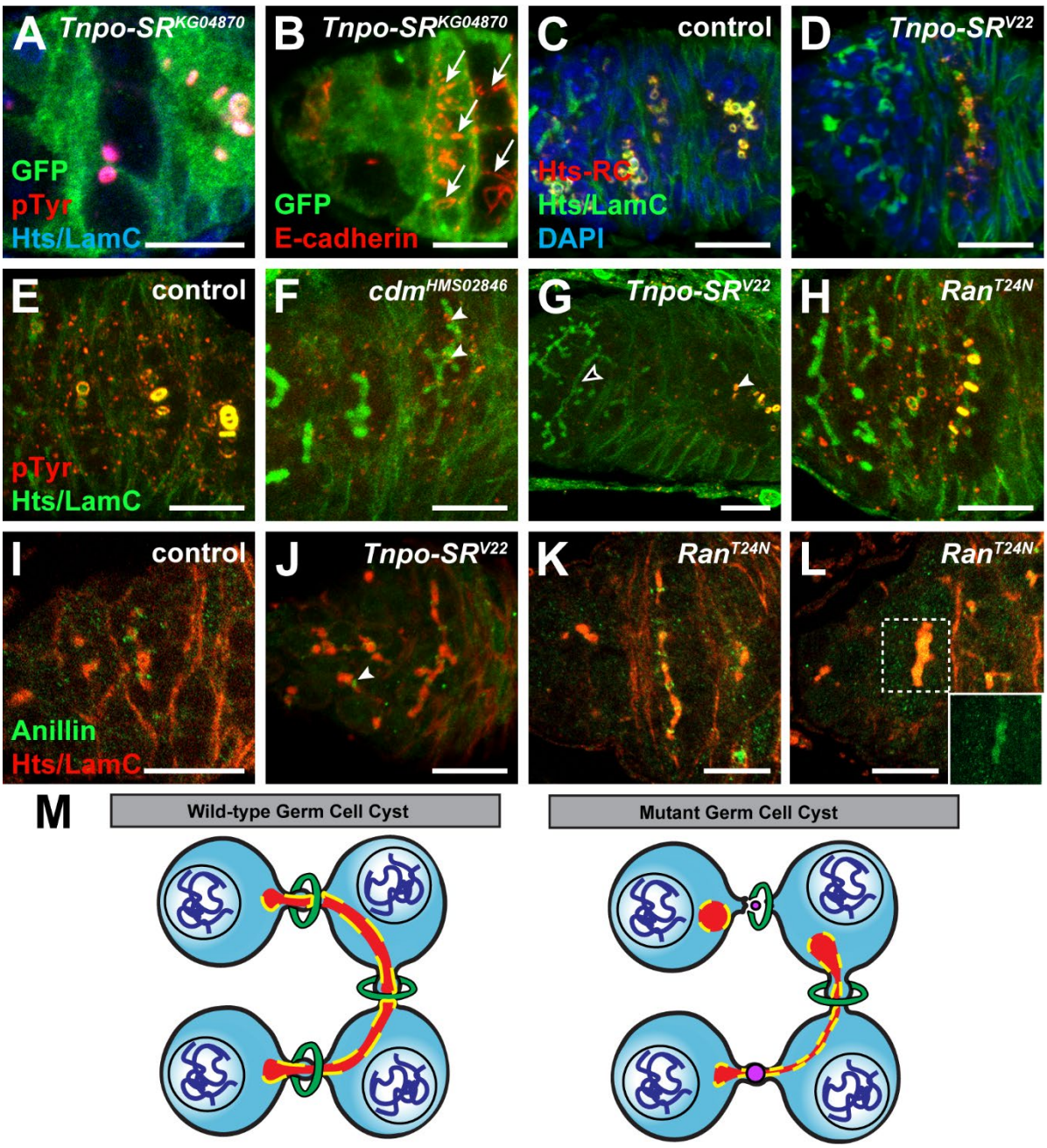

Figure 6. Depletion of *Tnpo-SR* and *cdm*, but not Ran-GTP, delays ring canal protein deposition and fails to suppress cytokinesis in dividing cysts.

(A) *Tnpo-SR*^{KG04870} mutant mosaic germarium labeled with anti-GFP (green; wild-type cells), anti-pTyrosine (pTyr, red), anti-Hts (blue), and anti-LamC (blue). (B) Maximum intensity projection of a *Tnpo-SR*^{KG04870} mutant mosaic germarium labeled with anti-GFP (green; wild-type cells) and anti-E-cadherin (red). Arrows indicate E-cadherin connections. (C-D) Control (C) and *nos-Gal4>Tnpo-SR*^{V22} (D) germaria labeled with Hts-RC (red), anti-Hts (green), anti-LamC (green),

928 and DAPI (blue). (E-H) Maximum intensity projections of driver control (E) and RNAi-depleted
929 *cdm* (F), *Tnpo-SR* (G), and *Ran* (H) cysts labeled with anti-pTyr (red), anti-Hts (green), and anti-
930 LamC (green). Arrowheads indicate ring canals; open arrowheads indicate a cyst lacking ring
931 canals. (I-L) Control (I), *nos-Gal4>Tnpo-SR*^{V22} (J) and *nos-Gal4>Ran*^{T24N} mutant (K-L)
932 germarium labeled with anti-anillin (green) anti-Hts (red), and anti-LamC (red). Arrowheads
933 indicate closed ring canals. Scale bars, 10 µm. (M) Summary of fusome and ring canal phenotypes
934 in *Tnpo-SR*- and *cdm*-depleted germ cell cysts.

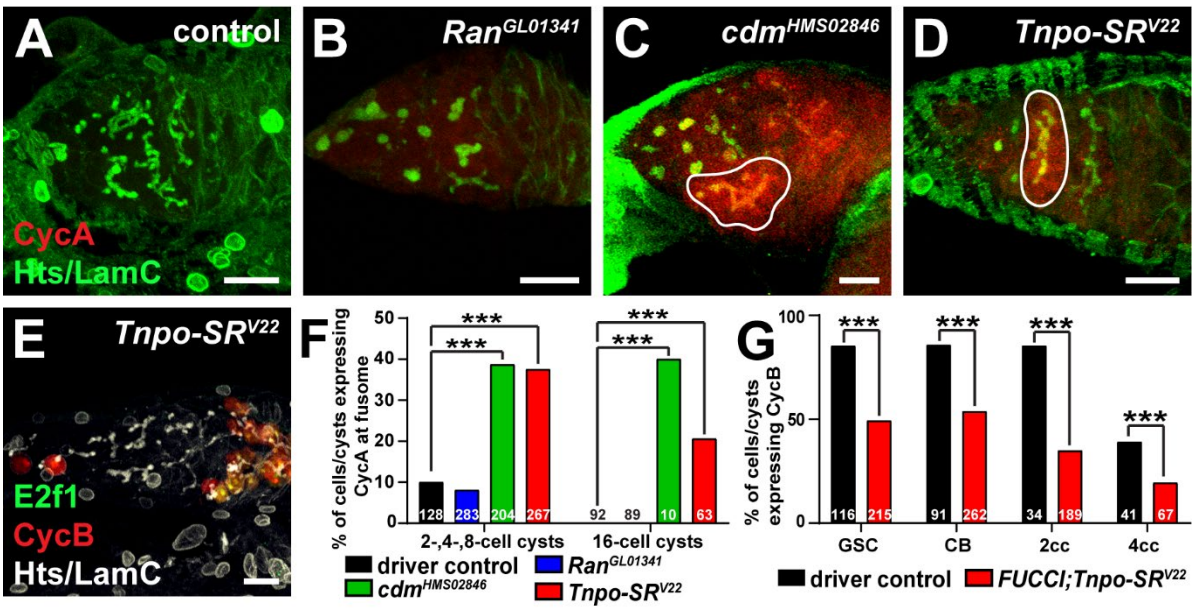

935

936 **Figure 7. CycA is ectopically expressed in c*dm* and *Tnpo-SR* cysts.**

937 (A-D) Driver control (A), *Ran*^{GL01341} (B), *cdm*^{HMS02846} (C), and *Tnpo-SR*^{V22} (D) RNAi knock-down
938 germaria labeled with anti-CycA (red), anti-Hts (green), and anti-LamC (green). (E) *nos-*
939 *Gal4>FUCCI;Tnpo-SR*^{V22} labeled with anti-GFP (green; E2f1), anti-dsRed (red; CycB), anti-Hts
940 (white), and anti-LamC (white). All images are maximum intensity projections. Scale bars, 10 µm.
941 (F) Percentage of cells/cysts containing fusome-localized CycA. (G) Percentage of cells/cysts
942 containing *RFP::CycB* in *nos-Gal4* controls and *Tnpo-SR*^{V22} knock-down germaria. The number
943 of cells/cysts analyzed is shown above bars. ***$p < 0.001$, Student's Chi-squared test.

944 **SUPPLEMENTAL DATA**

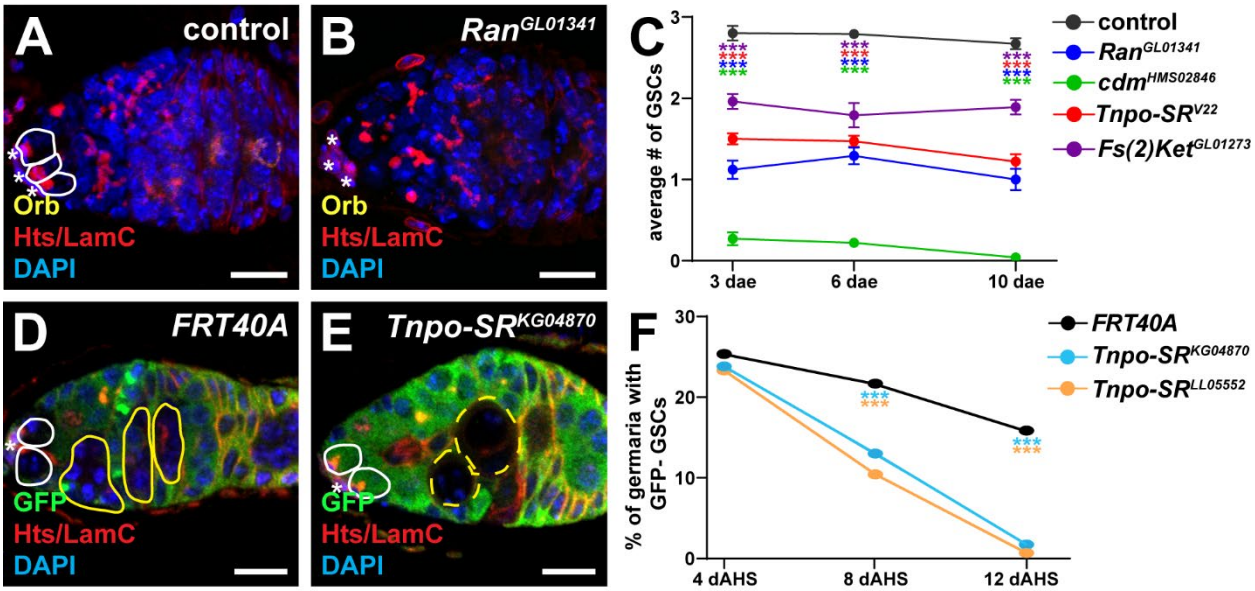

945

946 **Supp. Figure 1. Ran and β-importins are necessary for GSC maintenance.**

947 (A-B) *nos-Gal4* control (A) and *nos-Gal4>Ran*^{GL01341} (B) germaria labeled with anti-Orb (yellow),
948 anti-Hts (red), anti-LamC (red) and DAPI (blue). Solid white lines demarcate GSCs present in the
949 germarium, asterisks indicate cap cells. (C) Average number of GSCs per germarium in *nos-Gal4*
950 control or *nos-Gal4>UAS-Ran/importin RNAi* ovaries at 3, 6, and 10 days after eclosion (dae). At
951 least 30 germaria were analyzed at each timepoint. (D-E) *FRT40A* control (D) and *Tnpo-SR*^{KG04870}
952 *FRT40A* mutant (E) mosaic germaria at 8 days after clone induction labeled with anti-GFP (green),
953 anti-Hts (red), anti-LamC (red) and DAPI (blue). Lines demarcate wild-type (solid) or mutant
954 (dashed) GSCs (white) and cystoblast/cysts (yellow). (F) Percentage of total germaria analyzed
955 with a GFP-negative GSC at 4, 8, and 12 days after clone induction. At least 145 germaria were
956 analyzed for each genotype at each timepoint.

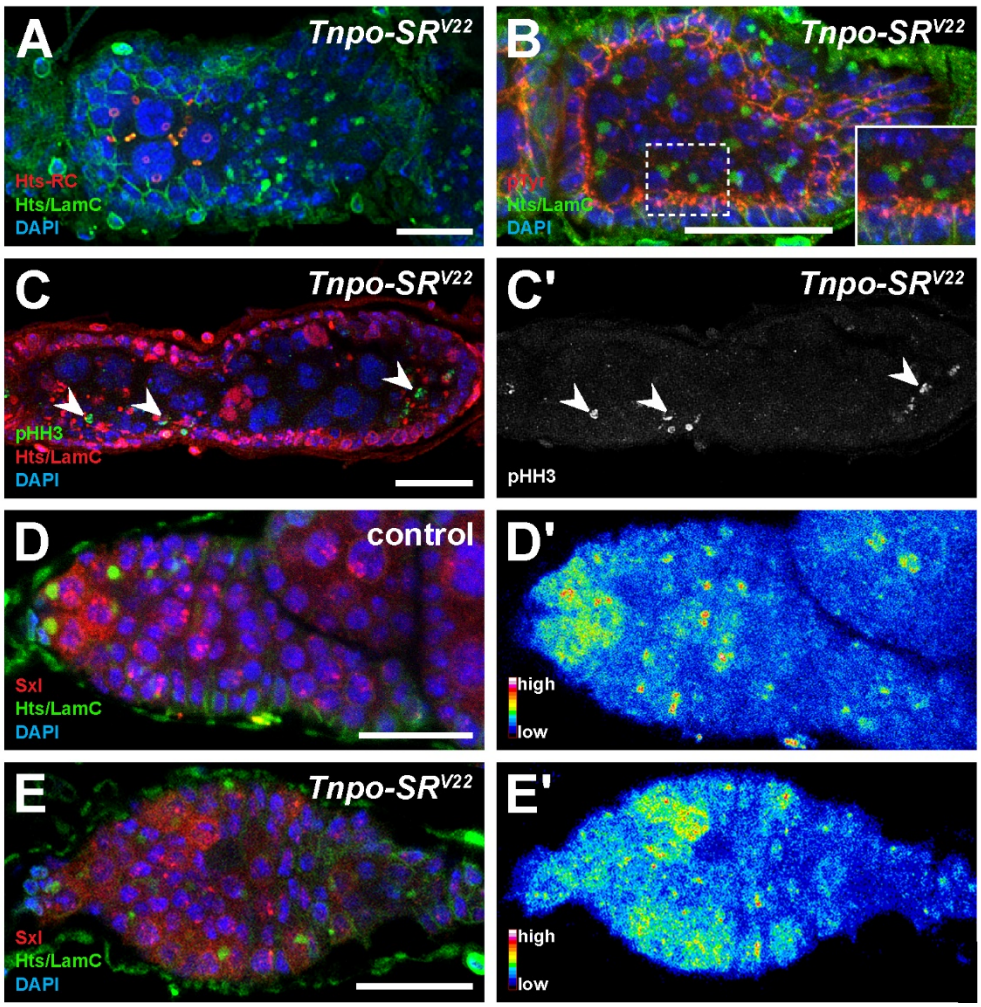

Supp. Figure 2. *Tnpo-SR* germline tumors are primarily composed of mitotically-dividing undifferentiated germ cells.

(A) *nos-Gal4>Tnpo-SR*^{V22} egg chamber labeled with anti-Hts-RC (red), anti-Hts (green), anti-LamC (green), and DAPI (blue). (B) *nos-Gal4>Tnpo-SR*^{V22} egg chamber labeled with anti-pTyr (red), anti-Hts (green), anti-LamC (green), and DAPI (blue). (C-C') *nos-Gal4>Tnpo-SR*^{V22} egg chamber labeled with anti-pHH3 (green), anti-Hts (red), anti-LamC (red), and DAPI (blue). Panel C' depicts pHH3 channel only. Arrowheads indicate pHH3-positive cells within the germline tumor. (D-E) Control (D-D') and *nos-Gal4>Tnpo-SR*^{V22} (E-E') germaria labeled with anti-Sxl (red), anti-Hts (green), anti-LamC (green), and DAPI (blue). Panels D' and E' show heat maps corresponding to panels D and E, where cool colors are low expression and warm colors are high expression. Scale bars, 20 µm.

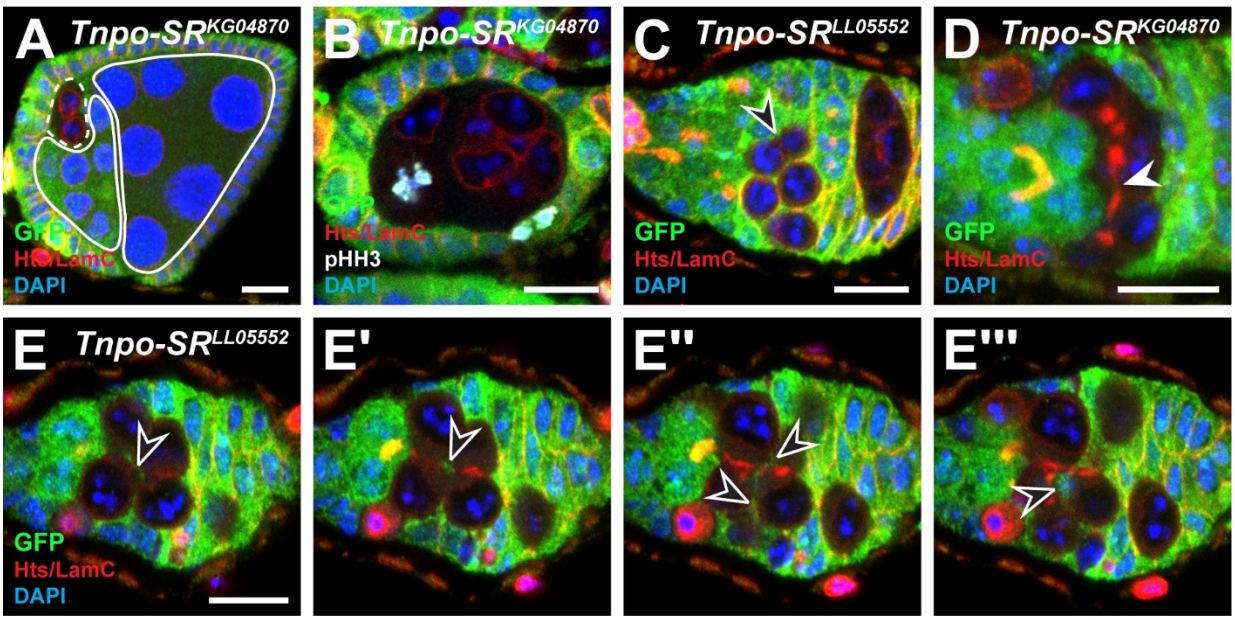

969

970 **Supp. Figure 3. *Tnpo-SR* mutants fail to maintain cyst connectivity and some cells are**
971 **ectopically mitotically active.**

972 (A) *Tnpo-SR*^{KG04870} mutant egg chamber labeled with anti-GFP (green), anti-Hts (red), anti-LamC
973 (red), and DAPI (blue). White lines indicate wild-type cysts (solid) and mutant cysts (dashed). (B)
974 *Tnpo-SR*^{KG04870} mutant egg chamber labeled with anti-GFP (green), anti-pHH3 (white), anti-Hts
975 (red), anti-LamC (red), and DAPI (blue). (C-E''') *Tnpo-SR*^{LL05552} (C and E-E''') and *Tnpo-*
976 *SR*^{KG04870} (D) mutant germaria labeled with anti-GFP (green), anti-Hts (red), anti-LamC (red), and
977 DAPI (blue). Panels E-E''' are adjacent 1 µm optical sections from the same germarium.
978 Arrowhead indicates thin thread of fusome material; open arrowheads follow the GFP+ somatic
979 cell projections invaginating the mutant cysts. (D) is a 2 µm subset maximum intensity projection.
980 Scale bars, 10 µm.

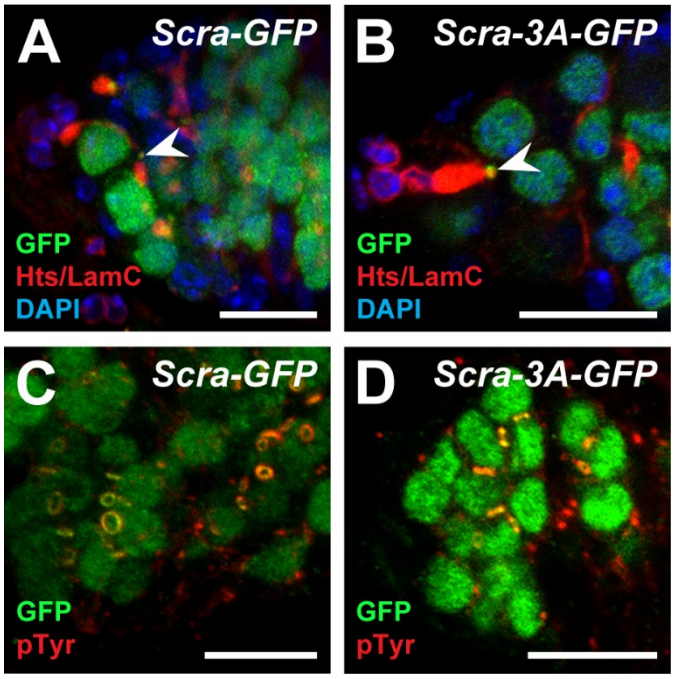

Supp. Figure 4. An Anillin-NLS mutant is not efficient in disrupting Anillin localization to nuclei and ring canals.

(A-D) Representative controls of *UAS-Scra-GFP* (A and C) and NLS mutated *UAS-Scra-3A-GFP* mutant (B and D) germaria labeled with anti-GFP (green), anti-Hts (red), anti-LamC (red), and DAPI (blue) (A-B) or anti-pTyrosine (red) (C-D). Arrowheads indicate closed ring canals. Scale bar, 10 µm.

988 **Supp. Table S1.** Fly stocks and immunofluorescence reagents used in this study.

Reagent	Source	Reference
nos-GAL4::VP16-nos.UTR	D. Drummond-Barbosa	(Rørth, 1998; Van Doren et al., 1998)
w; nosGal4::VP16, UASp-tubGFP*	BLM #7253	(Grieder et al., 2000)
$y^1sc^*v^1$; P{y[+t7.7] v[+t1.8]=TnpoSR-V22}attP2	Ables Lab	this study
y^1v^1; P{y[+t7.7] v[+t1.8]=TRiP.GL01483}attP2	BLM #43142	(Perkins et al., 2015)
$y^1sc^*v^1sev^{21}$; P{y[+t7.7] v[+t1.8]=TRiP.GL01341}attP40	BLM #42482	(Perkins et al., 2015)
$y^1sc^*v^1sev^{21}$; P{y[+t7.7] v[+t1.8]=TRiP.HMS02846}attP2	BLM #44551	(Perkins et al., 2015)
y^1v^1; P{y[+t7.7] v[+t1.8]=TRiP.HMS00020}attP2	BLM #33626	(Perkins et al., 2015)
$y^1sc^*v^1sev^{21}$; P{y[+t7.7] v[+t1.8]=TRiP.HMS01408}attP2	BLM #34998	(Perkins et al., 2015)
$y^1sc^*v^1sev^{21}$; P{y[+t7.7] v[+t1.8]=TRiP.HMS00991}attP2	BLM #34021	(Perkins et al., 2015)
y^1v^1; P{y[+t7.7] v[+t1.8]=TRiP.GL01273}attP2	BLM #41845	(Perkins et al., 2015)
y^1sc^*v1; P{y[+t7.7] v[+t1.8]=TRiP.HMS02968}attP2	BLM #50732	(Perkins et al., 2015)
$y^1sc^*v^1sev^{21}$; P{y[+t7.7] v[+t1.8]=TRiP.GL00435}attP40	BLM #35598	(Perkins et al., 2015)
$y^1sc^*v^1sev^{21}$; P{y[+t7.7] v[+t1.8]=TRiP.HMC03738}attP40	BLM #55142	(Perkins et al., 2015)
y^1v^1; P{y[+t7.7] v[+t1.8]=TRiP.HMJ22418}attP40/CyO	BLM #58311	(Perkins et al., 2015)

$y^1sc^*v^1sev^{21}$; P{y[+t7.7] v[+t1.8]=TRiP.HMC04414}attP40	BLM #56974	(Perkins et al., 2015)
y^1v^1; P{y[+t7.7] v[+t1.8]=TRiP.HMJ23009}attP40	BLM #61230	(Perkins et al., 2015)
hsFLP; FRT40A, UbiGFP / CyO	D. Drummond-Barbosa	(Ables et al., 2016)
FRT40A / CyO	D. Drummond-Barbosa	(Ables et al., 2016)
$y^{d2}w^{1118}$ P{ry[+t7.2]=ey-FLP.N}2 P{ry[+t7.2]=GMR-lacZ.C(38.1)}TPN1; P{y[+mDint2] w[BR.E.BR]=SUPor-P}Trn-SR[KG04870] P{ry[+t7.2]=neoFRT}40A / CyO, y[+]	Kyoto #111581	(Bellen et al., 2004; Chen et al., 2005)
y^*w^*; PBac{SAstopDsRed}LL05552 P{ry[+t7.2]=neoFRT}40A P{w[+mW.hs]=FRT(w[hs])}G13 cn^1bw^1 / CyO, S^*bw^1	Kyoto #141628	(Schuldiner et al., 2008)
w;P{UASp:Ran^{HA}}1.19/SM6	K. McKim	(Cesario and McKim, 2011)
w;P{UASp:Ran^{HA}}10-A/TM3	K. McKim	(Cesario and McKim, 2011)
w;P{UASp:Ran^{T24NHA}}18.3/TM3	K. McKim	(Cesario and McKim, 2011)
w;P{UASp:Ran^{T24NHA}}25.1/TM3	K. McKim	(Cesario and McKim, 2011)
w;P{UASp:Ran^{Q69LHA}}7.1/TM3	K. McKim	(Cesario and McKim, 2011)
w;P{UASp:ran^{Q69LHA}}61.2/TM3	K. McKim	(Cesario and McKim, 2011)
w[1118]; P{UASp-GFP.E2f.1-230}26 P{UASp-mRFP1.NLS.CycB.1-266}4/CyO,P{en1}wg[en11];MKRS/TM6B, Tb1	BLM #55110	(Zielke et al., 2014)
Rtnl1-GFP	B. Riggs, K. Röper	(Röper, 2007)

scrib^{CA07683}	L. Cooley, M. Buszczak	(Buszczak et al., 2007)
w**; P{w[+mC]=UASp-GFP-scra}3*	BLM #51348	(Silverman-Gavrila et al., 2008)
w**; wg*$^{Sp-1}$*/CyO; P{w[+mC]=UASp-GFP-3A-scra}3*	BLM #51347	(Silverman-Gavrila et al., 2008)

989